



Modeling of geophysical derived parameters for groundwater potential zonation using GIS-based multi-criteria conceptual model

Sunday Bayode¹ · Kehinde Anthony Mogaji¹ · Olakunle Egbeyemi¹

Received: 7 April 2021 / Accepted: 16 November 2023 / Published online: 12 January 2024
© The Author(s) 2024

Abstract

This study modeled geophysical derived parameters and multi-critically synthesized their themes based on geospatial and analytical hierarchy processes (AHP) approaches for groundwater potentiality prediction mapping. These methodologies were investigated in a typical hard rock geologic terrain, southwestern, Nigeria. Considering the spatially acquired 96 vertical electrical sounding (VES) data in the area, geoelectric sections revealing five subsurface layers including the topsoil, laterite, weathered layer, fractured basement and fresh basement rock were produced mindful of the 2-D resistivity structure subsurface imaging data interpreted results. The correlative results of the 2-D resistivity structure images and VES data interpretation results delineated major low resistivity vertical discontinuity typical of fractured zones characterized with width range of 25–40 m, while the depth vary from about 40 to >60 m. Themes of groundwater potential conditioning factors (GPCFs), namely: regolith, bedrock relief, hydraulic head, coefficient of anisotropy, aquifer resistivity and aquifer thickness were prepared from the re-analyzed hydrogeological and geophysical data. The produced themes were appropriately weighted in the context of AHP data mining technique. The groundwater potential prediction index (GPPI) mathematical modeling equation for the area was established via applying the weight linear average algorithm involving the AHP weight-age results. The synthesized results of the applied GPPI model equation on the GPCFs' hydrogeologic themes give GPPI values in the range 1.59–3.65 for the study area. The geospatial modeling of the GPPI estimated values result produced groundwater potential prediction index map for the area. The produced GPPI model map zoned the area into low (1.59–2.30), medium (2.30–2.61), medium–high (2.61–3.02) and high (3.02–3.65) groundwater potential classes. The area analysis of the GPPI map indicates that more than 70% of the study area has 'low to medium groundwater potential. The GPPI map result verification using reacting operating characteristics technique results gave 86% and 81% success and prediction rates, respectively. The findings of this study are useful to water managers and decision-makers for locating appropriate positions of new productive wells in the study area and other areas with similar geologic settings.

Keywords Groundwater potentiality prediction index · GIS · Geoelectric · Analytical hierarchy process · ROC · Hard rock terrain

Introduction

The typical characteristic of an urban area is its rapid growth in population and high industrialization (Todd and Mays 2005; Magesh et al. 2012; Adiat et al. 2013; Oikonomidis et al. 2015) and these have often resulted to increase in urban water demands (Mukherjee et al. 2009). Apart from the insufficiency of surface water resource being the most available and renowned major sources of water supply in both urban and rural areas, the impact of the industrial technological advancement resulting to climatic change effect has also reduced the surface water freshness reliability and sustainability (Graham-Tomasi and Yacov 2004; Abdulla and

✉ Kehinde Anthony Mogaji
kamogaji@futa.edu.ng
Sunday Bayode
sbayode@futiebodea.edu.ng
Olakunle Egbeyemi
egbeyemiolaunle@yahoo.com

¹ Department of Applied Geophysics, Federal University of Technology, P.M.B. 704, Akure, Nigeria

Al-Shareef 2009). Consequently, these have aroused challenges and a threat to global water security (UNESCO and UNESCO-WSSM 2019). In order to address this impending global water crisis, the attentions toward the development of groundwater resources as alternative to surface water resource have been on the increase (Vörösmarty et al. 2010; Marsalek et al. 2006; George et al. 2009). According to several researchers, groundwater is one of the most important natural resources for providing freshwater sources worldwide (Pham et al. 2019). This could probably due to groundwater resources' unique attributes such as: good quality, constant temperature, low vulnerability to pollution, and low susceptibility to catastrophic events (Chowdhury et al. 2009). However, groundwater is a hidden natural resource, whose occurrences and accumulation in an area varies largely from one place to another (Adiat et al. 2012; Akinlalu et al. 2017; Mogaji and Lim 2017). Hence, to optimize groundwater resources exploration, the need arises for carrying out comprehensive hydrogeologic, geophysical evaluation and geospatial modeling assessment for these important resources irrespective of any geological setting of interest.

The renowned conventional approach for developing groundwater resources is via borehole drilling and some other hydrogeologic means. Nevertheless, these aforementioned techniques are uneconomical (Todd 1980; Roscoe Moss Co. 1990; Fetter 1994) due to high cost of drilling, time-consuming, labor intensive, destructive and lack of regionalized predictive assessment. In alternative, the methodological approaches involving geophysical and geospatial and data mining techniques according to Madan et al. (2010). Mogaji (2016) can largely addressed these shortcomings.

Thus, this study explored the state-of-the-art approach involving geospatial and data mining modeling techniques with the view of proposing a conceptualized data mining indexing algorithm to maximize groundwater resource development in this problematic geologic terrain effectively is timely. Among the renowned data mining technique in the field of groundwater hydrology, the AHP-MCDA is the most prominent in the field of groundwater hydrology. This is probably because the AHP method has a robust capability for the conjunctive and integrated analysis of multidisciplinary data sets (Chowdhury et al. 2010). Arising from previous works, the efficacy of application of GIS-based AHP method to endogenous induced groundwater potentiality condition factors (GPCFs) in the field of groundwater hydrology is relatively limited. In accordance with Jha et al. (2010), the endogenous factors are in situ subsurface lithology physical properties that have direct bearing with groundwater accumulation and movement.

This study is aimed at delineation of potential groundwater zones using hydrogeologic and geophysical data that are obtainable from the analyzed primary and secondary

geolectric parameters (Dar Zarrouk parameters) namely: regolith variation, groundwater head, hydraulic head, and coefficient of anisotropy, aquifer resistivity and aquifer thickness. These multi variables GPCFs will be multi-criterially synthesized based on the established groundwater potential prediction index (GPPI) mathematical modeling equation. Exploring the unique in situ physical properties of the endogenous data from which aquifer hydraulic parameters can be quantitatively determined will largely established a wider application of AHP technique of MCDA method in the field of groundwater hydrology. Thus, this research output will give a broader perspective of developing a more efficient and reliable decision support system model whose output will provide technical support to government agencies as well as private sectors for groundwater development decision-making and assessment in the investigated area.

Description of the study area

Geography, geology, and hydrogeology

The area studied falls within the South-western part of Nigeria. It is situated between $7^{\circ} 18' 6''$ to $7^{\circ} 18' 43''$ Latitudes and $5^{\circ} 13' 16''$ to $5^{\circ} 14' 18''$ Longitudes with an area extent coverage of about 2 km^2 (Fig. 1). The topographic elevation of the area ranges from 301 to 412 m a.m.s.l. The average annual rainfall amount characterizing the area is about 1333.2 mm (NIMETS 2011). The geologic setting of the area falls within the Precambrian Basement Complex of southwestern Nigeria (Rahaman 1976). Though, based on the geological field survey carried out, the pronounced lithological unit among others is the charnockite rock. Thus, this area can be inferred to be a monolithic geologic setting (Fig. 1). A charnockitic rocky unit is known for undergoing spheroidal weathering, whose end product often resulted in clay lithology with little or no evidence of fracture development (Keller and Frischnecht 1966). However, according to Satpathy and Kanungo (1976) and Lewis (1990), the basement terrain aquifer is not only inhomogeneous but also occurs in a discrete and discontinuous manner. In crystalline rock terrains, the weathered layer and the fractured basement rocks constitute the main hydrogeologic units. However, significant amount of water can be stored in the weathered layer/fractured basement rock aquifer units when the thickness is sufficiently high Bayode (2013).

Methodology

Geophysical survey

Geoelectrical survey was deployed along Six (6) traverses of 260–660 m established in an approximately E–W direction

Fig. 1 Location, geological and data acquisition map of the study area

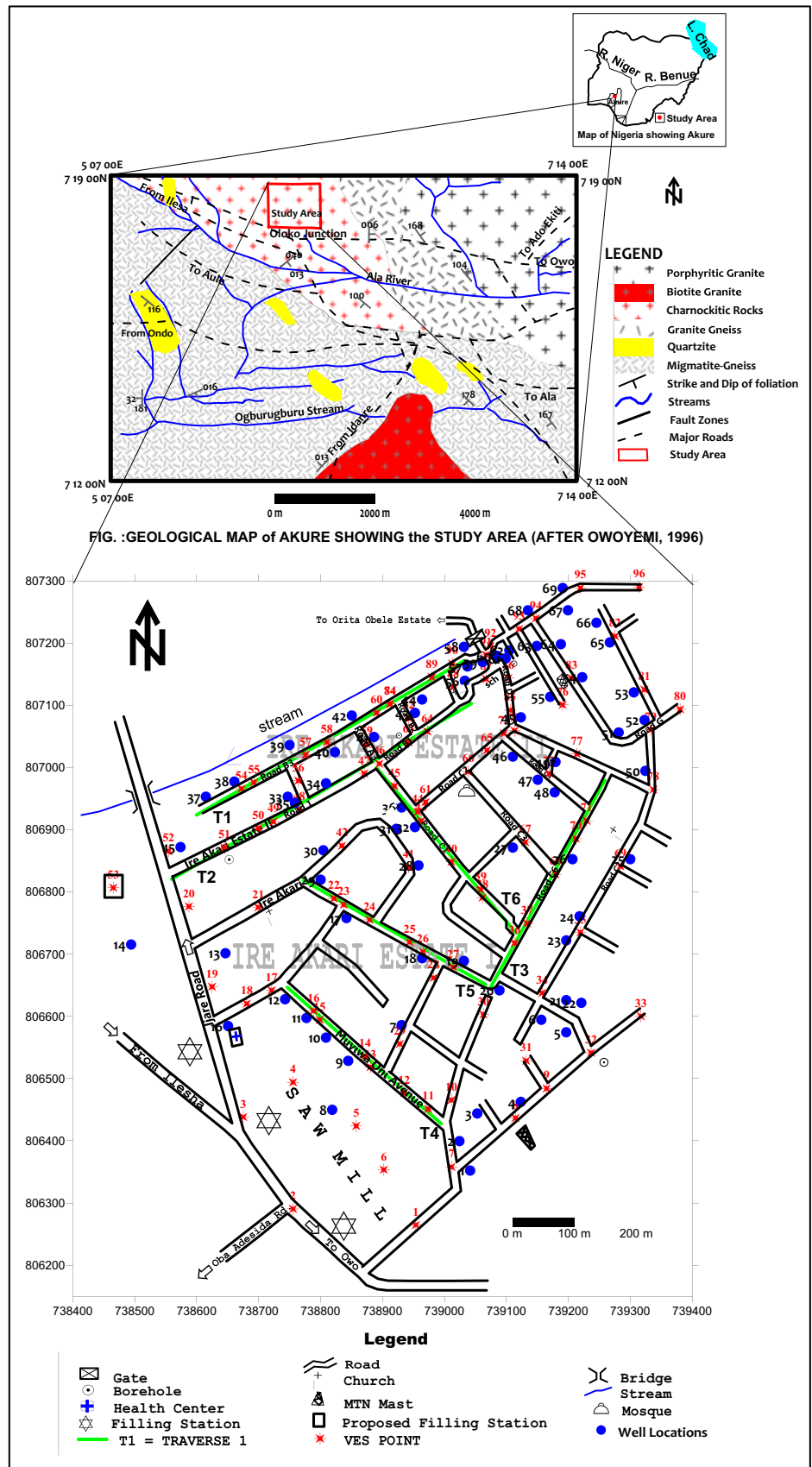


(Fig. 1). The geoelectrical measurement was carried out adopting the dipole–dipole profiling technique in the company of vertical electrical sounding (VES) technique as a followed up. The combined 2-D subsurface imaging and 1-D VES measurement approaches often allow delineation of subsurface geologic structures as well as mapping of the continuous vertical, horizontal variation of resistivity within the subsurface and for subsurface lithologic correlation with the geoelectric sections. On the established 2-dipole–dipole traverses, measurements were made at electrode spacing of $a=20$ m and expansion factor n , varying from 1 to 5. The acquired dipole–dipole data were inverted into a 2-D resistivity structure using the DIPRO for windows (2000) software. Upon the 2-D subsurface imaging resistivity structure interpretation, 5–9 VES measurements were carried out along the traverses. Figure 2 presents a typical 2-D resistivity structure with the VES location. In this study, the remaining VES stations were approximately evenly distributed along roads and other available spaces across the study area. A total of ninety-six (96) VES measurements were carried out engaging the Ohmega resistivity meter across the investigated area. Among the observed data, were some parametric sounding measurements as typify at VES 48 location, purposely for lithologic correlation and data interpretation constraint. The acquired 1-D VES data were interpreted following the standard partial curve matching technique coupled with the use of the Win RESIST 1.0 (Vender Velper 2004) software for the 1-D forward modeling. Presented in (Fig. 3) are the representatives VES data interpreted resistivity curves. Based on this interpretation was the determined primary layer geoelectric parameters such as resistivities (r) and thicknesses (h) which were further processed and used to generate both 1-D subsurface geoelectric sections as well as the secondary geoelectric parameter modeling (The Dar-Zarrouk parameters). Typical of the produced 1-D subsurface geoelectric section is shown in Fig. 4. Besides, the generated secondary geoelectric parameters include Transverse unit resistance (T) and longitudinal unit conductance (S) from which the coefficient of Anisotropy (λ) was evaluated.

Hydrogeologic investigation

A hydrogeologic study involving depth to water level (DWL) assessment from the accessible hand-dug wells in the area was carried out involving the use of measuring tape, etc. Showing in (Fig. 1) are the located sixty-five (65) wells occupied in the area. Two seasons including the wet season (at the peak of the raining season in August, 2011) and dry season (at the peak of the dry season in February, 2012) were considered for the hydrogeologic measurement. The record of the hydrogeological measurement is presented in Table 2.

Modeling of groundwater potential conditioning factors (GPCFs)

In line with several researchers, the concepts of deriving either subsurface or surface-induced aquifer potential controlled factors have greatly enhanced groundwater resources development in diverse geological terrains (Adiat et al. 2013; Akinlalu et al. 2017; Mogaji and Lim 2018). Thus, this study derived possible groundwater potential influencing factors using the processed geophysical and hydrogeological data acquired. The brief of the procedural approach for the considered vital parameters modeling is as highlighted:

Re-analysis of geoelectrical properties for Dar Zarrouk parameters modeling

The Dar Zarrouk parameters (DSPs) have its fundamental basis from the determined primary geoelectrical parameters such as resistivity and thickness obtainable from the interpreted geophysical data (Table 1). In accordance with Tizro et al. (2010), Oborie and Udom (2014) and Mogaji (2017), the Dar Zarrouk parameter is the secondary parameter indices derived from the determined primary geoelectrical parameters. According to Oladapo et al. (2009), the varying subsurface layer/lithological layer are often inferred from the aforementioned primary geoelectrical parameters. Nominally, the DSPs are the longitudinal unit conductance (S), the transverse unit resistance (T), the average longitudinal resistivity (ρ_L) and the average transverse resistivity (ρ_T). The hybrid re-analysis of S , T , λ , ρ_L and ρ_T is considered in modeling of coefficient of anisotropy (λ) parameter (A). The λ can be defined for a geoelectric section consisting of several (n) layers of a unit cube of rock with the total thickness (H). The degree of subsurface fracturing or inhomogeneity can be established through the determination of electrical coefficient of anisotropy (λ) particularly, in a typical basement complex terrain, where permeability is enhanced by faults, fractures, joints and shear zones. In the studies of Olorunfemi et al. (1991), Bayode and Akpoarebe (2011) and Ojo et al. (2015), the above-mentioned geological significance of faults, fractures, joints and shear zones largely enhanced groundwater yield of an area. Thus, the concept of modeling the coefficient of anisotropy (λ) in the area will largely contribute to its groundwater potentiality assessment. Mathematically, the S and T parameters can be defined by Eqs. 1 and 2 (Keller and Frischnecht 1966):

$$\rho_T = \frac{T}{H} \quad (1)$$

$$\rho_L = \frac{H}{S} \quad (2)$$

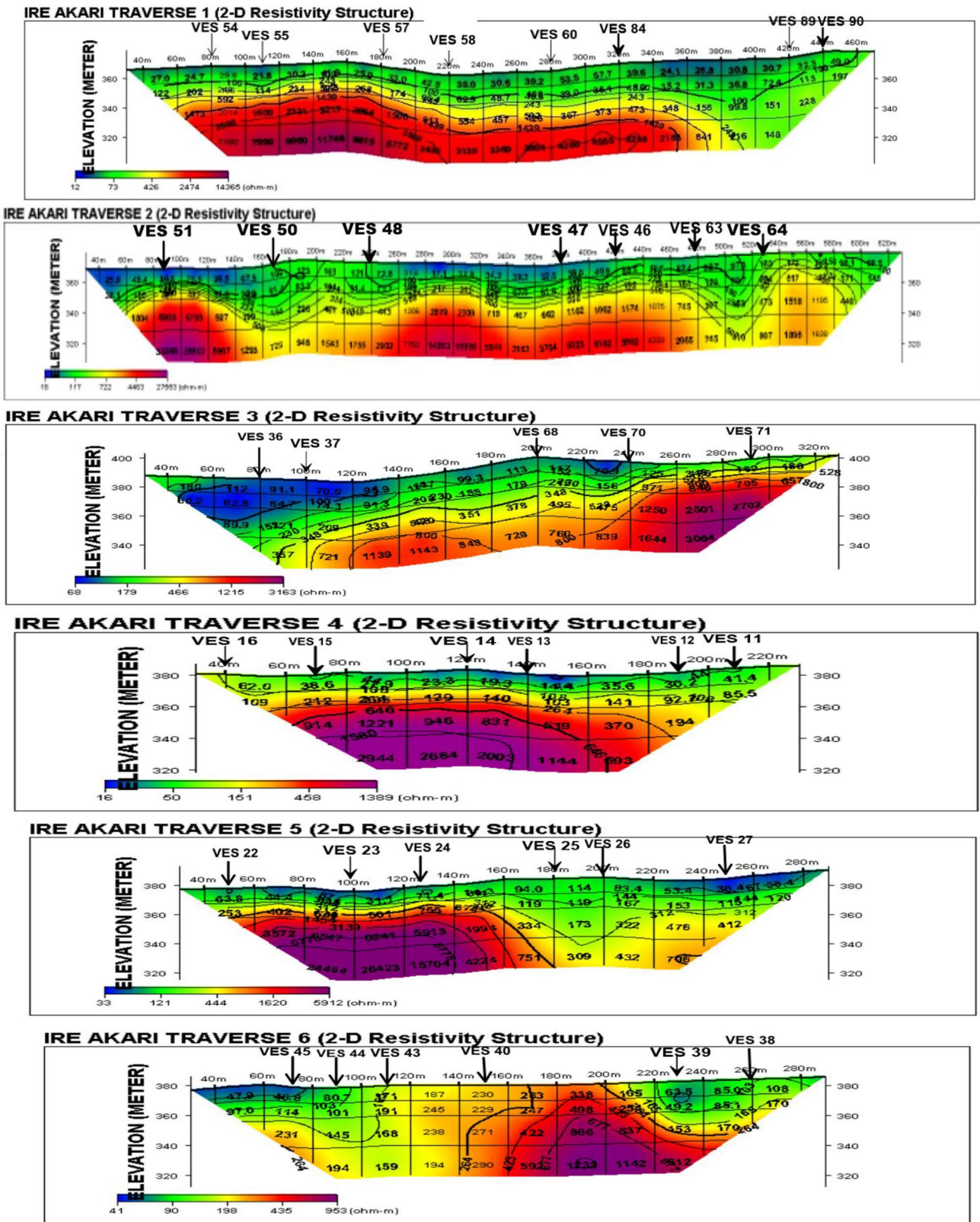


Fig. 2 The inverted 2-D resistivity structure images generated for the established traverses 1–6

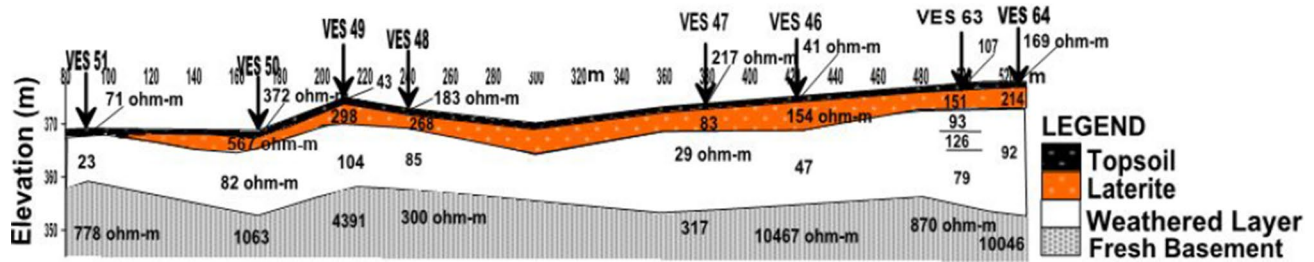


Fig. 3 Typical 2-D geoelectric section generated in the area

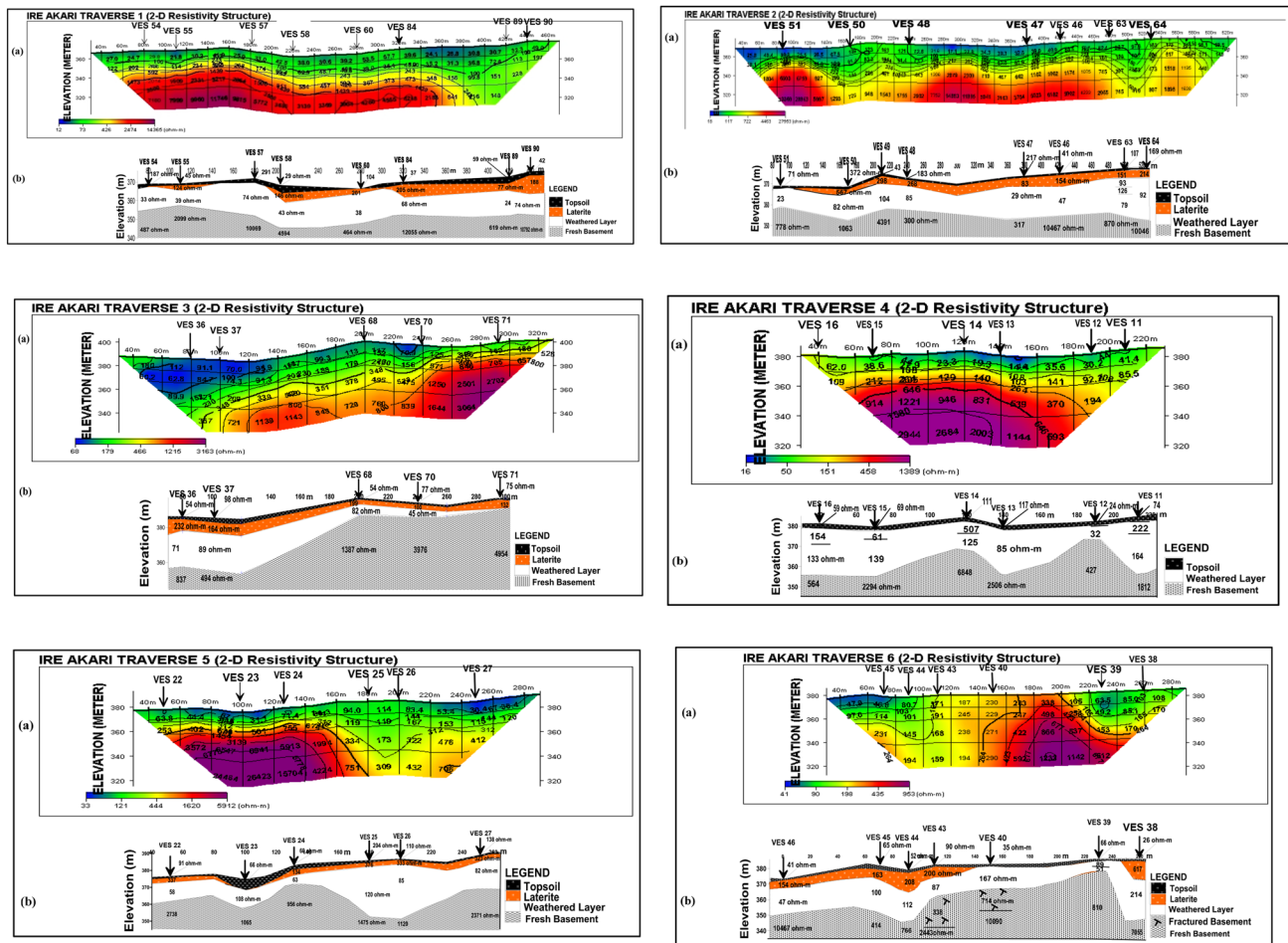


Fig. 4 The correlative panel results for the 2-D profiling and 1-D geoelectrical imaging across traverses 1–6

$$\lambda = \sqrt{\frac{\rho_T}{\rho_L}} \tag{3}$$

$$\lambda = \frac{\sqrt{TS}}{H} \tag{4}$$

The inputs from Eqs. 1 and 2 are engaged in Eqs. (3) and (4) to define the coefficient of anisotropy (λ) parameter for the area subsurface lithology.

The hydrogeologic parameter modeling

The subsurface data were hydrogeologically observed from the available hand dug wells. On each located wells, the depth to water level (DWL) below ground surface is

Table 1 The result summary of the geophysical data interpretation

VES no	Easting	Northing	Resistivity (Ohm-m) $\rho_1/\rho_2/\dots/\rho_n$				Thickness (m) $h_1/h_2/\dots/h_3$			
1	738,953.8074	806,264.548	192	565	51	656	0.9	4.1	23.9	
2	738,755.5693	806,290.3702	81	250	96	3174	1.3	8.5	26.4	
3	738,675.1248	806,438.131	104	339	163	704	0.7	6	14.5	
4	738,755.5693	806,494.0793	69	56	139	2274	1.4	2.5	18.3	
5	738,857.5614	806,423.7853	103	150	65	1548	1.5	2	19.2	
6	738,902.0931	806,353.4913	156	539	147	1189	1.8	6.2	29.7	
7	739,011.2678	806,357.7951	25	104	52	1672	0.6	7	7.4	
8	739,114.6964	806,436.6965	126	32	862		1.4	4.9		
9	739,164.9742	806,484.0373	81	131	57	2650	0.8	2.1	7.7	
10	739,011.2678	806,465.3879	97	176	96	382	1	2.4	28.2	
11	738,973.9186	806,451.0422	74	222	164	1882	1	10.6	14.4	
12	738,935.1328	806,476.8644	24	32	427		0.9	6.3	8	
13	738,880.5455	806,518.467	117	85	2506		4.9	18.3		
14	738,871.9265	806,535.6818	111	507	125	6848	1	4.7	8.1	
15	738,798.6645	806,594.4992	69	61	139	2294	1.6	2.9	19.8	
16	738,788.609	806,608.845	59	155	133	564	1.5	6.5	19.3	
17	738,721.0931	806,641.8401	59	25	1840		1.5	5.8		
18	738,680.8708	806,620.3215	68	113	35	1143	1.4	10.5	17.7	
19	738,624.847	806,647.5784	62	166	143	250	1.9	10	13.5	
20	738,587.4978	806,776.6897	96	154	63	462	2.1	9.6	13.0	
21	738,699.5454	806,775.2552	69	56	139	2274	1.4	2.5	18.3	
22	738,821.6487	806,789.6009	91	117	58	2738	0.5	2.4	12.4	
23	738,837.4502	806,779.5589	66	108	1065		4.9	17.6		
24	738,879.109	806,755.1712	69	134	63	956	0.6	3.3	5.7	
25	738,943.7519	806,719.3069	204	376	120	1475	1.2	4.2	26.6	
26	738,965.2995	806,703.5266	110	333	85	112	0.7	2.5	26.6	
27	739,014.1408	806,679.1389	138	323	82	2371	0.6	2.6	18.9	
28	738,982.5376	806,661.9241	189	442	223	5995	1.0	5.5	7.3	
29	738,927.9503	806,555.7658	55	87	3421		3.4	5.9		
30	739,062.9821	806,603.1067	63	163	126	375	2.0	12.2	16.0	
31	739,131.9345	806,528.509	93	88	954		2.9	2.5		
32	739,236.7996	806,541.4201	198	448	242	2612	1.1	8.9	9.3	
33	739,317.2441	806,600.2375	87	361	143	1751	1.5	9.8	13.5	
34	739,157.7916	806,637.5364	96	161	103	11,634	1	6.1	10.6	
35	739,219.5615	806,735.0872	66	116	41	1177	1.3	9	22.1	
36	739,113.2599	806,717.8723	54	232	71	837	0.7	6.4	16.5	
37	739,133.371	806,749.4329	98	164	89	494	2.6	7	21.4	
38	739,061.5456	806,791.0354	26	617	214	7055	0.6	11.3	23.3	
39	739,058.6725	806,803.9466	66	59	51	810	1.5	4.5	6.2	
40	739,011.2678	806,848.4183	35	167	714	10,090	0.7	5.4	9.4	24.1
41	738,942.3154	806,839.8109	61	49	3848		1.4	5.2		
42	738,834.5772	806,874.2406	32	102	111	1145	0.6	4.8	10.5	
43	738,962.4265	806,914.4085	90	200	87	328	1.3	4.8	6.4	35
44	738,956.6805	806,928.7542	52	208	112	766	1.1	10.4	19.4	
45	738,919.3312	806,970.3568	65	163	100	414	0.7	6.4	15.7	
46	738,894.9106	807,006.2211	41	154	47	10,467	0.6	3.6	15.9	
47	738,870.4899	806,990.4408	217	83	29	317	0.8	4.0	3.1	
48	738,765.6248	806,933.058	183	268	85	300	1.1	1.8	12.8	
49	738,723.9661	806,912.974	43	298	104	4391	0.8	4.4	12.3	
50	738,699.5454	806,902.932	372	567	82	1063	0.9	2.3	12.6	

Table 1 (continued)

VES no	Easting	Northing	Resistivity (Ohm-m) $\rho_1/\rho_2/\dots/\rho_n$					Thickness (m) $h_1/h_2/\dots/h_3$					
51	738,644.9581	806,871.3714	71	23	778				1.3	8.5			
52	738,554.4581	806,865.6331	38	13	2773				1.5	5.8			
53	738,465.3946	806,806.8157	83	140	60	8913			1.1	1.4	6.4		
54	738,672.2518	806,966.0531	187	33	487				1.5	12.4			
55	738,692.3629	806,976.0951	45	124	39	2099			0.7	2.7	9.6		
56	738,764.1883	806,978.9642	60	183	71				0.6	4.1	16.8		
57	738,775.6804	807,020.5668	291	74	10,069				2.9	19.2			
58	738,810.1566	807,040.6508	29	146	43	4594			0.6	4.5	13.2		
59	738,874.7995	807,037.7816	80	168	84	2443			1.2	5	11.8		
60	738,890.6011	807,087.9916	104	291	38	464			0.7	1.9	17.1		
61	738,969.609	806,944.5345	63	278	137	2599			1.1	6.2	7.7		
62	738,942.3154	807,079.3842	53	279	171	2565			0.9	7.4	9.5		
63	738,942.3154	807,040.6508	107	151	93	126	79	870	1	0.8	2.4	3.5	3.3
64	738,972.482	807,057.8656	169	214	92	10,046			1	2.9	20.7		
65	739,068.7281	807,027.7396	102	214	129	911			0.8	6.2	10.6		
66	739,038.5614	806,993.3099	146	22	305				1.1	4.7			
67	739,130.498	806,879.9788	114	83	148	75	933		1.1	2	3.7	7.5	
68	739,179.3393	806,828.3343	54	199	82	1387			0.5	2.5	6.7		
69	739,284.2044	806,841.2454	367	117	1047				2.3	9.8			
70	739,212.379	806,885.7171	77	100	45	3976			0.9	2.5	3.4		
71	739,229.6171	806,914.4085	75	132	4954				0.9	4.9			
72	739,169.2837	806,990.4408	82	134	119	30,060			1.3	5.8	22.9		
73	739,096.0218	807,054.9965	129	154	74	505			0.8	1.8	4		
74	738,912.1487	807,102.3373	43	540	1505				2.4	4.8			
75	739,113.2599	807,059.3002	227	416	102	2616			1.8	4.4	23.5		
76	739,190.8313	807,100.9027	283	246	88	1431			0.9	8.9	11.5		
77	739,213.8155	807,022.0013	69	117	51	198			1.5	8.2	21.4		
78	739,337.3552	806,964.6185	568	250	49	5759			1.5	5.1	18.6		
79	739,333.0457	807,060.7348	114	248	86	1676			0.5	2.2	8.7		
80	739,380.4504	807,093.7299	72	610	1188				1.2	6.6			
81	739,322.9901	807,125.2904	88	230	94	2122			0.5	3.1	18.8		
82	739,275.5853	807,211.3647	75	124	82	418			0.8	10.1	17.6		
83	739,205.1964	807,143.9399	34	204	58	2128			1.1	10.5	20.4		
84	738,923.6	807,109	37	205	68	12,055			0.8	5.6	13.8		
85	739,106.0773	807,092.2953	255	65	2829				4.1	15.3			
86	739,103.2043	807,143.9399	135	441	71	10,143			0.7	3.3	14.3		
87	739,067.2916	807,142.5053	140	141	357	11,468			0.8	7.7	17.0		
88	739,014.1408	807,129.5942	90	193	99	1446			1.3	8.5	26.4		
89	738,979.6646	807,145.3744	59	77	24	619			0.7	6	14.5		
90	739,012.7043	807,166.893	42	188	74	10,792			1.4	2.5	18.3		
91	739,067.2916	807,181.2387	246	275	78	4963			1.5	2	19.2		
92	739,074.4741	807,195.5844	44	98	34	389			1.8	6.2	29.7		
93	739,120.4424	807,222.8413	28	171	108	10,111			0.6	7	7.4		
94	739,147.7361	807,240.0561	27	40	658				1.4	4.9			
95	739,219.5615	807,288.8315	179	83	32	952			0.8	2.1	7.7		
96	739,314.3711	807,290.2661	54	159	111	1251			1	2.4	28.2		

Table 2 The observed well measurement

Well no	Easting	Northing	Elevation	DWL (m) wet season	DWL (m) dry season	Hydraulic head
1	739,041.4	806,352.1	387.0	6.67	7.2	380.33
2	739,024.2	806,399.4	390.2	7.2	8.3	383.0
3	739,052.9	806,443.9	393.0	5.5	7.2	387.5
4	739,123.3	806,462.5	397.0	4.5	5.6	392.5
5	739,196.6	806,574.4	387.0	7.2	7.8	379.8
6	739,156.4	806,594.5	375.7	7.3	9.0	368.4
7	738,930.8	806,585.9	380.0	8.7	8.75	371.3
8	738,844.6	806,528.5	335.0	7.19	9.3	327.81
9	738,808.7	806,565.8	366.0	7.2	9.95	358.8
10	738,777.1	806,597.4	363.0	7.45	8.95	355.55
11	738,742.6	806,627.5	341.1	7.25	Dry	333.85
12	738,650.7	806,584.5	329.0	3.02	3.4	325.98
13	738,841.8	806,758	329.7	6.9	7.2	322.8
14	738,963.9	806,693.5	350.3	7.1	7.9	343.2
15	739,031.4	806,689.2	379.0	7.2	7.25	371.8
16	739,088.8	806,641.8	350.5	7.32	8.2	343.18
17	739,196.6	806,626.1	383.0	4.75	7.05	378.25
18	739,221	806,621.8	389.0	7.5	9.0	381.5
19	739,196.6	806,722.2	394.0	8.72	Dry	385.28
20	739,218.1	806,760.9	329.0	8.8	9.85	320.2
21	739,300	806,852.7	349.0	8.4	Dry	340.6
22	739,206.6	806,852.7	396.0	5.15	5.5	390.85
23	739,110.4	806,871.4	381.0	6	Dry	375.0
24	738,958.1	806,842.7	361.0	6.15	7.65	354.85
25	738,800.1	806,819.7	351.0	6.17	6.2	344.83
26	738,804.4	806,867.1	333.8	5.8	6.0	328.0
27	738,922.2	806,901.5	380.0	5.45	6.15	374.55
28	738,952.4	806,904.4	363.0	6.4	8.2	356.6
29	738,747	806,953.1	361.0	5.04	6.0	355.96
30	738,808.7	806,974.7	372.0	3.8	5.45	368.2
31	738,758.4	806,943.1	360.0	3.95	7.5	356.05
32	738,930.8	806,935.9	363.0	5.6	7.05	357.4
33	738,614.8	806,953.1	373.0	3.13	4.0	369.87
34	738,660.8	806,977.5	353.0	2.9	3.4	350.1
35	738,749.8	807,036.3	361.0	1.3	1.8	359.7
36	738,823.1	807,024.9	363.0	4.0	4.8	359.0
37	738,886.3	807,049.3	360.0	5.7	6.1	354.3
38	738,850.4	807,083.7	374.0	3.7	4.15	370.3
39	738,952.4	807,088	377.0	6.2	7.7	370.8
40	738,963.9	807,109.5	353.0	4.8	6.1	348.2
41	739,123.3	807,080.8	380.0	8.0	8.75	372.0
42	739,110.4	807,017.7	372.0	6.5	7.5	365.5
43	739,150.6	806,980.4	364.0	8.5	9.6	355.5
44	739,177.9	806,960.3	363.0	9.2	8.7	353.8
45	739,179.3	807,009.1	367.0	8.75	9.6	358.25
46	739,324.4	806,994.7	382.0	9.3	10.3	372.7
47	739,281.3	807,056.4	387.0	8.8	9.2	378.2
48	739,323	807,076.5	390.0	9.0	9.8	381.0
49	739,305.8	807,121	391.0	9.9	10.7	381.1
50	739,222.4	807,145.4	385.0	6.7	8.0	378.3

Table 2 (continued)

Well no	Easting	Northing	Elevation	DWL (m) wet season	DWL (m) dry season	Hydraulic head
51	739,170.7	807,113.8	387.0	8.0	9.05	379.0
52	739,032.8	807,139.6	380.0	5.6	6.55	374.4
53	739,037.1	807,162.6	333.0	5.9	6.45	327.1
54	739,031.4	807,194.1	337.0	3.1	3.2	333.9
55	739,061.5	807,169.8	343.0	4.7	5.7	338.3
56	739,084.5	807,179.8	361.0	5.6	7.7	355.4
57	739,098.9	807,175.5	369.0	6.6	7.3	362.4
58	739,104.6	807,188.4	373.0	7.0	8.6	366.0
59	739,149.2	807,195.6	382.0	5.6	7.0	376.4
60	739,188	807,198.5	386.0	5.3	6.8	380.7
61	739,267	807,201.3	392.0	8.0	9.3	384.0
62	739,245.4	807,232.9	381.0	5.9	7.1	375.1
63	739,199.5	807,253	383.0	3.0	4.8	380.0
64	739,134.8	807,253	380.0	4.4	5.25	375.6
65	739,190.8	807,288.8	375.0	1.9	2.75	373.1

DWL depth to water level

measured using measuring tape. In order to determine the height (H) of the groundwater table above mean sea level in each hand dug well, a similar approach adopted in the study of Acharya et al. (2017) was used. This entails, subtraction of DWL value from the in situ observed height on the ground surface above mean sea level recorded by the GPS device at each occupied location. As explained in the study of Ge and Gorelick (2015), “ H ” is one of the key variables in describing a groundwater system. In the same study, the Hydraulic head (H) has been defined as a fundamental parameter in describing groundwater flow in rocks. It is a function of the ratio of mechanical energy to the unit weight of fluid in the aquifer system because water flows between two points in response to unequal distributions of the water’s mechanical energy. In the present study, hydraulic head (H) for the study area was computed considering the DWL readings observed during wet season (Column 5 of Table 2) and surface elevation measurements undertaken for the 65 wells occupied. Using Eq. (5), the degree of hydraulic head (H) variation for the area was computed.

$$H = \text{EASL} - \text{DWL} \quad (5)$$

Regolith (Re) parameter modeling

The term Regolith (Re) is synonymous to overburden that described all the materials which overlie the bedrock. Assessing this parameter often gives insight into knowing the sizable column thickness of weathered materials characterizing the layers including vadose zone, aquifer unit, etc. In accordance with Olorunfemi, et al. (1999), Bala and Ike (2001) and Bayode (2018), practical evaluation of “Re”

parameter can be used in the hydrogeological investigation. For the ‘Re’ parameter modeling, the acquired depth sounding or VES data were processed and interpreted for subsurface lithological units delineation (Table 3). The encompassing lithological materials occasioned at varying depth to the bedrock beneath each occupied VES locations were summed up to determine the ‘Re’ variation in the investigated area.

Bedrock relief (B) parameter modeling

The insight into knowing the nature and subsurface topographic configuration characterizing an area has often been defined by the bedrock relief (B) variation (Omosuyi et al. 2007; Bayode et al. 2017; Adagunodo et al. 2018). Studies have established that the estimation of “B” parameter often varied from one place to another (Mogaji 2016; Omosuyi et al. 2007). This variation largely depends on the geological setting and the degree of weathering depth experienced in an areas. The variations in the degree of B in a typical hard rock terrain is determined by the intense of tectonic activity resulting to faults, fractures, joints, etc. occurring in such geological terrain. To model the “B” parameter, the geoelectrical layer thickness for the regolith materials and the corresponding terrain topographic elevation variation measurement were considered. In the area, the terrain topography elevation was observed using the integrated topographic map of the area and the standard GPS instrument measurement, while the regolith thickness was determined from the processed and interpreted VES geophysical data.

Table 3 The geoelectrical-based GPCFs modeled results

VES no.	Easting	Northing	Re (m)	<i>B</i>	<i>A</i>	<i>R</i>	<i>T</i>
1	738,953.8074	806,264.548	28.9	353.10	1.46	616	28.0
2	738,755.5693	806,290.3702	36.2	315.80	1.09	346	34.9
3	738,675.1248	806,438.131	21.3	313.70	1.06	502	20.5
4	738,755.5693	806,494.0793	22.2	316.80	1.05	195	20.8
5	738,857.5614	806,423.7853	22.7	337.30	1.03	215	21.2
6	738,902.0931	806,353.4913	37.7	334.30	1.12	686	35.9
7	739,011.2678	806,357.7951	15.0	378.00	1.08	156	14.4
8	739,114.6964	806,436.6965	6.3	394.70	1.17	32	4.9
9	739,164.9742	806,484.0373	10.6	380.40	1.06	188	9.8
10	739,011.2678	806,465.3879	35.9	353.10	0.31	704	30.6
11	738,973.9186	806,451.0422	26.0	359.00	1.04	354	25.0
12	738,935.1328	806,476.8644	15.2	365.80	1.02	76	14.3
13	738,880.5455	806,518.467	23.2	350.80	1.2	516	18.3
14	738,871.9265	806,535.6818	13.8	371.20	1.02	64	12.8
15	738,798.6645	806,594.4992	24.3	348.70	1.05	200	22.7
16	738,788.609	806,608.845	10.0	371.00	1.01	128	10.0
17	738,721.0931	806,641.8401	7.2	367.80	1.06	25	5.8
18	738,680.8708	806,620.3215	29.6	318.40	1.16	148	28.2
19	738,624.847	806,647.5784	25.4	321.60	1.03	309	23.5
20	738,587.4978	806,776.6897	17.0	343.00	1.06	229	15.5
21	738,699.5454	806,775.2552	22.2	338.80	1.05	195	20.8
22	738,821.6487	806,789.6009	13.5	364.50	1.2	294	13.0
23	738,837.4502	806,779.5589	22.5	335.50	1.17	461	17.6
24	738,879.109	806,755.1712	9.6	374.40	1.07	197	9.0
25	738,943.7519	806,719.3069	9.2	377.80	1.06	249	8.4
26	738,965.2995	806,703.5266	5.1	356.90	1.16	231	4.1
27	739,014.1408	806,679.1389	22.1	368.90	1.11	405	21.5
28	738,982.5376	806,661.9241	13.8	358.20	1.17	353	10.8
29	738,927.9503	806,555.7658	8.6	374.40	1.03	37	3.3
30	739,062.9821	806,603.1067	42.8	325.20	1.08	707	41.6
31	739,131.9345	806,528.509	5.4	391.60	1.0	88	2.5
32	739,236.7996	806,541.4201	19.3	376.70	1.05	690	18.2
33	739,317.2441	806,600.2375	24.8	387.20	1.12	504	23.3
34	739,157.7916	806,637.5364	17.6	357.40	1.02	264	16.7
35	739,219.5615	806,735.0872	32.4	328.60	1.11	157	31.1
36	739,113.2599	806,717.8723	29.5	356.50	1.09	297	28.8
37	739,133.371	806,749.4329	31.0	354.00	1.03	253	28.4
38	739,061.5456	806,791.0354	35.2	350.80	1.21	831	34.6
39	739,058.6725	806,803.9466	12.2	373.80	1.03	140	10.7
40	739,011.2678	806,848.4183	32.8	350.20	1.11	474	31.4
41	738,942.3154	806,839.8109	6.5	357.50	1.0	49	5.2
42	738,834.5772	806,874.2406	15.9	333.10	1.03	213	15.3
43	738,962.4265	806,914.4085	25.0	357.00	1.02	311	23.7
44	738,956.6805	806,928.7542	30.9	345.10	1.06	324	29.8
45	738,919.3312	806,970.3568	22.8	360.20	1.03	263	22.1
46	738,894.9106	807,006.2211	20.1	352.90	1.11	201	19.5
47	738,870.4899	806,990.4408	14.6	355.40	1.13	99	13.6
48	738,765.6248	806,933.058	15.7	357.30	1.08	353	14.6
49	738,723.9661	806,912.974	17.5	357.50	1.14	340	16.7
50	738,699.5454	806,902.932	15.8	352.20	1.31	649	14.9
51	738,644.9581	806,871.3714	9.8	359.20	1.08	23	8.5

Table 3 (continued)

VES no.	Easting	Northing	Re (m)	<i>B</i>	<i>A</i>	<i>R</i>	<i>T</i>
52	738,554.4581	806,865.6331	7.3	358.70	1.1	13	5.8
53	738,465.3946	806,806.8157	8.9	353.10	1.05	200	7.8
54	738,672.2518	806,966.0531	13.9	355.10	1.17	33	12.4
55	738,692.3629	806,976.0951	13.0	356.00	1.11	163	12.3
56	738,764.1883	806,978.9642	21.6	350.40	1.07	254	20.9
57	738,775.6804	807,020.5668	22.1	351.90	1.12	74	19.2
58	738,810.1566	807,040.6508	18.3	345.70	1.15	189	17.7
59	738,874.7995	807,037.7816	18.0	353.00	1.05	252	16.8
60	738,890.6011	807,087.9916	18.7	344.30	1.19	244	18.2
61	738,969.609	806,944.5345	19.1	360.90	1.05	246	17.9
62	738,942.3154	807,079.3842	17.9	366.10	1.08	450	16.9
63	738,942.3154	807,040.6508	21.0	356.00	1.02	449	20.0
64	738,972.482	807,057.8656	24.5	353.50	1.04	306	23.6
65	739,068.7281	807,027.7396	17.6	379.40	1.03	343	16.8
66	739,038.5614	806,993.3099	5.8	381.20	1.32	22	4.7
67	739,130.498	806,879.9788	14.3	369.70	1.04	306	13.2
68	739,179.3393	806,828.3343	9.7	387.30	1.09	281	9.2
69	739,284.2044	806,841.2454	12.1	340.90	1.11	117	9.8
70	739,212.379	806,885.7171	6.8	386.20	1.07	145	5.9
71	739,229.6171	806,914.4085	5.8	391.20	1.02	132	4.9
72	739,169.2837	806,990.4408	30.0	334.00	1.0	253	28.7
73	739,096.0218	807,054.9965	6.6	393.40	1.06	228	5.8
74	738,912.1487	807,102.3373	7.1	400.90	1.83	540	4.8
75	739,113.2599	807,059.3002	29.7	358.30	1.14	518	27.9
76	739,190.8313	807,100.9027	21.3	370.70	1.14	334	20.4
77	739,213.8155	807,022.0013	31.1	345.90	1.07	168	29.6
78	739,337.3552	806,964.6185	25.2	352.80	1.39	299	23.7
79	739,333.0457	807,060.7348	11.4	378.60	1.09	334	10.9
80	739,380.4504	807,093.7299	7.8	382.20	1.36	610	6.6
81	739,322.9901	807,125.2904	22.4	367.60	1.05	324	21.9
82	739,275.5853	807,211.3647	28.5	364.50	1.02	206	27.7
83	739,205.1964	807,143.9399	32.0	350.00	1.2	262	30.9
84	738,923.6	807,109	15.5	375.50	1.15	273	24.1
85	739,106.0773	807,092.2953	19.4	360.60	1.17	65	15.3
86	739,103.2043	807,143.9399	18.3	371.70	1.28	512	17.6
87	739,067.2916	807,142.5053	31.4	334.60	1.24	1641	30.8
88	739,014.1408	807,129.5942	8.7	373.30	1.05	292	8.0
89	738,979.6646	807,145.3744	19.5	352.50	1.13	101	17.2
90	739,012.7043	807,166.893	26.8	349.20	1.11	262	25.9
91	739,067.2916	807,181.2387	22.7	355.30	1.11	353	21.9
92	739,074.4741	807,195.5844	21.3	362.70	1.11	132	20.5
93	739,120.4424	807,222.8413	31.1	342.90	1.06	279	30.3
94	739,147.7361	807,240.0561	9.9	377.10	1.01	40	8.7
95	739,219.5615	807,288.8315	11.6	360.40	1.17	115	10.7
96	739,314.3711	807,290.2661	20.4	280.60	1.05	270	18.2

Re regolith, *B* bedrock relief, *A* coefficient of anisotropy, *R* aquifer resistivity, *T* aquifer thickness, *GPCFs* groundwater potentiality conditioning factors

Aquifer unit resistivity and thickness (*R*) and (*T*) parameters modeling

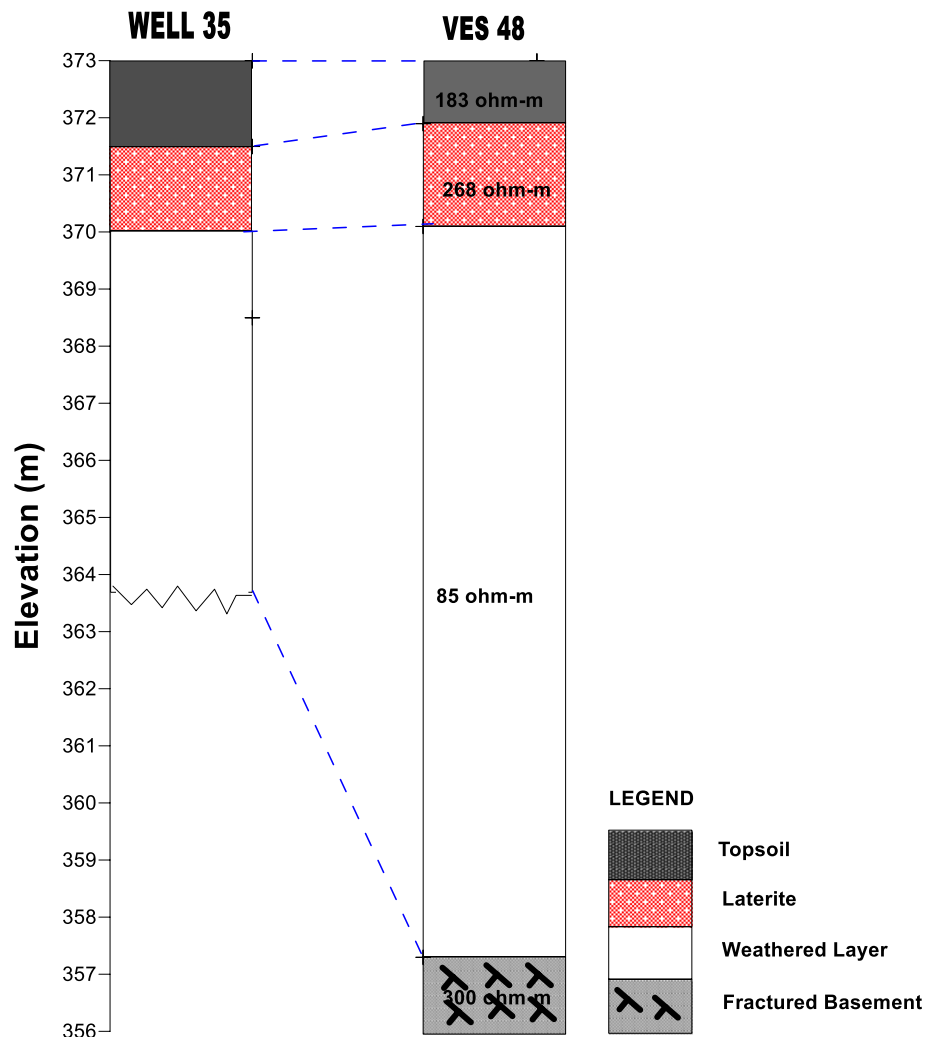
These parameters were modeled from the geoelectrical delineated subsurface lithologic units (Fig. 2). In a typical Basement Crystalline Terrain, the immediate layer above the possible bedrock is often referred to as the aquifer unit lithology. Considering the geoelectrical determined physical properties, such as resistivity and thickness of the delineated aquifer unit beneath each occupied VES locations (Table 1), both “*R*” and “*T*” parameters values were modeled/estimated, respectively. The records of the determined *R* and *T* are detailed in Table 3

Geospatial modeling of GPCFs’ themes and their hydrological significance

According to Table 3 records, numerical estimate of varying values was determined per VES location for the considered GPCFs in this study. Exploring the efficacy of GIS

technique, the georeferenced coordinates in columns 2 and 3 against their determined GPCFs continuous numerical values were processed to produce spatial model hydrologic themes. Figure 5 presents the generated hydrologic themes for the area. In the studies of Chowdhury et al. (2009), Adiat et al. (2013) and Nampak et al. (2014), some groundwater potentiality influencing factors similar to the above discussed GPCFs have been reported for their appeal hydrological relevance. The generated “*Re*” spatial model theme modeled from the *Re* determined values beneath the VES location (Table 3 and Fig. 5a) often depict zones of high and low *Re* variations. According to Bala and Ike (2001), Omosuyi et al. (2013) and Bayode (2018), such depicted high and low *Re* variation zones have found to be associated with areas of high and low groundwater potential in their previous studies. The implication of *B* parameter hydrogeologically is such that it has great influence on dischargeability, rechargeability, and storage of an aquifer unit and thus the fluid subsurface movement in and out of varying lithology is greatly controlled. The *B* parameter theme (Fig. 5b) was

Fig. 5 The hand dug well lithologic and parametric VES data interpretation correlation



generated via spatial modeling of the computed B values in Table 3. The “ H ” parameter spatially model in (Fig. 5c, Table 2) enables identifying zones of varying degrees of run-off viz-a-viz high or low variation. Its significance can be likened to water that naturally flows from a zone of high hydraulic head to a region of lower hydraulic head along a hydraulic gradient in the same manner in which heat would also flow toward lower temperature regions. Higher ranks were assigned to the regions with lower hydraulic head as compared to the zones with higher hydraulic heads was scored low. The nature and storativity potential of the area underlain and delineated aquifer units was spatially modeled (Fig. 5e and f) using the determined geoelectrical property values in columns 7 and 8 of Table 3. With the knowledge of the aquifer resistivity “ R ”, inference of the existence of a weathered, fractured, fault, jointed and sheared condition gives insight to the existence of conduit medium for surface water recharge while the thickness values “ T ” for this unit tells much about the available aquifer unit space for fluid accumulation and containment.

The applied multi-criteria decision methods (MCDMs) theory/principle

The basis of a multi-criteria modeling method revolved around the knowledge-driven expert and criteria analysis synthesis to aid planners and policy/decision-makers in environmental studies. In accordance with Malczewski and Rinner (2005) and Malczewski (2006), the challenges of spatial mapping involving a large set of feasible alternatives with multiple conflicting and incommensurate evaluation criteria have been effectively addressed using the MCDMs' algorithm. Typical of such MCDMs analyzed result has aided in natural/mineral resources precision and prediction modeling (De Araujo and Macedo 2002; Feizizadeh and Blaschke 2013; Al-Abadi and Shahid 2016). The two key processes involved in this study' MCDMs applied technique include (1) Normalized weighting assignment/Rating scores apportioning and (2) weight linear combination mechanism.

The normalized weighting assignment/rating scores apportioning

The considered GPCFs discussed in “Geospatial modeling of GPCFs' themes and their hydrological significance” section played an essential role in this index modeling. Each of these GPCFs' themes was assigned weight, depending on their influences on the groundwater potential prospect. For the effective weighting assignment, the analytical hierarchy processes (AHP) technique whose mechanism largely driven by the principle of Saaty's scale was adopted in this study. Using this Saaty's scale standard the Criteria Pair-wise Comparison Matrix Analysis of these GPCFs was generated. The

rating scores on other hand for each of the GPCFs' class boundaries regarding their contributing influence toward the aquifer expected productivity potential is based on the similar approach adopted in the study of Al-Saud (2010). According to Al-Saud (2010), the rating is basically numerical values in the range of 1–5, where (1) Very low, (2) Low, (3) Medium, (4) Medium–high and (5) High.

The AHP multi-criteria modeling theory

A good account of the analysis and the modeling theory of AHP technique has been reported in the studies of Chowdary et al. (2009), Madan et al. (2010), Machiwal et al. (2015), Adiat et al. (2012) and Mogaji and Lim (2017). However, below are some of the simple mathematical relationships that substantiate the uniqueness of the AHP MCDA method in terms of its capability to (or) measure the degree of consistency among the pairwise comparisons of contributing factors in decision making. Such sound mathematical basis equations can be defined as Eqs. 6 and 7 as reported in the studies of Adiat et al. (2012) and Thirumalaivasan et al. (2003):

$$CI = \frac{\lambda_{\max} - n}{n - 1} \quad (6)$$

$$CR = \frac{CI}{RI} \quad (7)$$

where CI: consistency index. This index determines the inconsistencies in the pair-wise judgments and is a measure of departure from consistency based on the comparison matrix developed. The λ_{\max} is the average value of the consistency vector and n is the number of criterion in the matrix (Vahidnia et al. 2009; Garfi et al. 2009). The CR is the ratio of the matrix, which shows the degree of consistency achieved when comparing the criteria or the probability that the matrix rating was randomly generated, whereas the RI is the random index. The value of the RI largely depends on the number of criteria being compared (Garfi et al. 2009).

The multi-criteria weight linear average technique application

The mechanism of weight linear average (WLA) according to Eastman (1996) is driven in terms of normalized weight of criteria and normalized scores/rating for all options relative to each of the GPCFs themes considered (Fig. 5). The WLA simple mathematical modeling expression is ably expressed in Eq. 8:

$$Y = \sum_{i=1}^n NW_i R_i \quad (8)$$

where Y is the expected output, NW_i : the normalized weighted value for each theme (Fig. 5) and R_i is the assigned score for the class boundary in each theme (criterion). The synthesis of the GPCFs' themes (Fig. 5), for developing groundwater potential prediction index modeling equation can be established through applying Eq. (8) algorithm.

The developed groundwater potential prediction index (GPPI) modeling equation

In order to establish a potentiality index modeling algorithm in this study, a multi-criteria synthesizing model is conceptualized for the purpose of combining the groundwater potential influencing factors obtainable from both hydrogeological and geophysical measurements. The proposed GPPI model mathematical equation explored the efficacy of the WLA and AHP weightage assessment techniques for the integration of both hydrogeo-physical electrical derived-based GPCFs. The regionalized capability of this developed groundwater potential prediction index (GPPI) model was effectively executed in the GIS platform. Referencing the established Eq. (8), the GPPI modeling algorithm can be developed as modified thus in Eq. 9.

$$GPPI = Re_{NW_i} Re_{X_i} + B_{NW_i} B_{X_i} + H_{NW_i} H_{X_i} + A_{NW_i} A_{X_i} + R_{NW_i} R_{X_i} + T_{NW_i} T_{X_i} \quad (9)$$

where Re : regolith; B : Bedrock relief; H : Hydraulic head; A : coefficient of anisotropy; R : aquifer Resistivity and T : aquifer thickness; NW : AHP-based normalized weight; R : rating GPPI: groundwater potential prediction index.

Results and discussion

2-D Resistivity structures and geoelectric sections results

The 2-D resistivity inversion assisted in imaging the subsurface geologic sequence, the attributes and the structural disposition of the geo-electric layers in the subsurface. Figure 2 presents the 2-D resistivity structures generated for the established traverses. Three subsurface geoelectric layers were delineated. The layers are generally classified as the topsoil/weathered layer, fractured basement and the fresh basement. Depth to topsoil and the weathered layer may have been merged because of overlapping resistivity values and the thickness of the topsoil. This geoelectric unit is characterized by light-deep bluish/greenish/yellowish-reddish color. The values of the resistivity range between 12 and 179 Ω m, while the thickness varies from 0.5 to 2.5 m. The top soil/weathered unit comprises clay, clayey sand, sand and laterite. The weathered layer is characterized by clay, sandy

clay, clayey sand and lateritic clay/lateritic concretion. Low resistivity values ranging from 12 to 100 Ω m are characterized as clay, while the resistivity values of 100–250 Ω m are interpreted as sandy clay and clayey sand units. The second layer, is denoted as the fractured basement layer. Its resistivity and thickness values generally range between 121 and 650 Ω m and about 25–> 40 m, respectively. Moreover, the depth ranges for the delineated fractured basement is about 40–> 60 m. Besides, the fractured basement is characterized by vertical discontinuity and break within the relatively resistive basement bed rock (between distances > 370 m; 480–530 m; 180–220 m; 90–120 m along traverses 1, 2, 5 and 6, respectively). The delineated fractured basement zones which are made up of partially weathered materials exhibits relatively low resistivity zones denoted by green color band overlapping the highly resistive basement host rock with depth extent greater than 60 m. Fresh basement bedrock is delineated as the last layer. It is characterized by yellowish–reddish color bands. The basement bedrock's resistivity generally ranges from 198 to ∞ Ω m along the six (6) traverses. The typical 2-D geoelectric section image produced based on the interpreted VES data along traverse T2 is presented in Fig. 4. The sections assisted in categoriz-

ing the area into five subsurface geologic layers/sequences. The correlation panel of the 2-D Resistivity Structures and 2-D Geoelectric Sections subsurface images along Traverses 1–6 is presented in Fig. 6. This figure shows that unlike the results obtained from the 2-D resistivity imaging of the subsurface, the geoelectric sections delineated five subsurface layers comprising the topsoil, laterite, weathered layer, fractured basement and the fresh basement bedrock. Table 4 contains the summary of the geoelectric parameters. The fractured basement is localized beneath VES 40 and 43.

Figure 7 presents the parametric sounding's result of interpretation obtained beside a located hand dug well in the study area. The figure equally shows the comparison between the hand-dug well section dug to a depth of 9.5 m and the columnar section for VES 48 which delineated a total depth to bedrock of 15.7 m within the investigated area. The lithologic correlation between the well log and the VES 48 interpretation result shows that the thickness of the lithologic units obtained for the well log are topsoil 1.5 m, laterite 1.5 m, weathered layer > 6.5 m while the VES delineated corresponding thicknesses of 1.1 m, 1.8 m, 12.8 m, respectively. Therefore, this correlation further confirmed the interpretation accuracy of the VES technique adopted and hence, its reliability in this work. The weathered layer and the fractured basement with relatively low resistivity values which range from 12–400 Ω m and 121–650 Ω m;

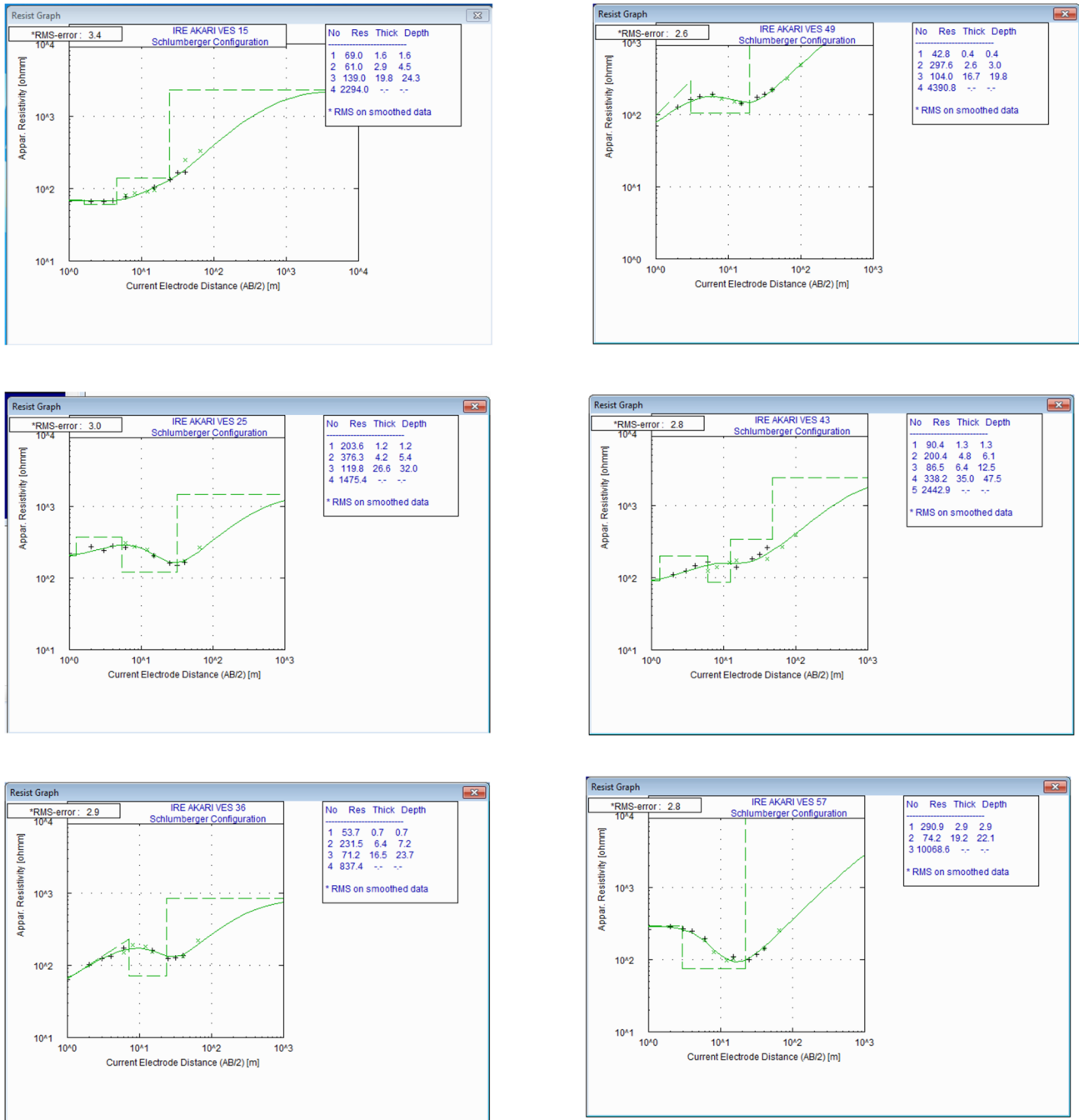


Fig. 6 Typical depth sounding curves obtained from the study area

Table 4 Geoelectric parameters beneath the study area

Layering	Resistivity range (Ω m)	Thickness (m)	Lithologic description
Topsoil	24–567	0.4–2.6	Clay, sandy clay, clayey sand and laterite
Laterite	77–617	1.8–17.6	Lateritic clay
Weathered layer	23–222	2.5–36.0	Clay and sandy clay
Fractured basement	338–714	4.8–35.0	Partly weathered/fractured basement
Basement bedrock	300– ∞	*5.4–37.7	Fresh basement

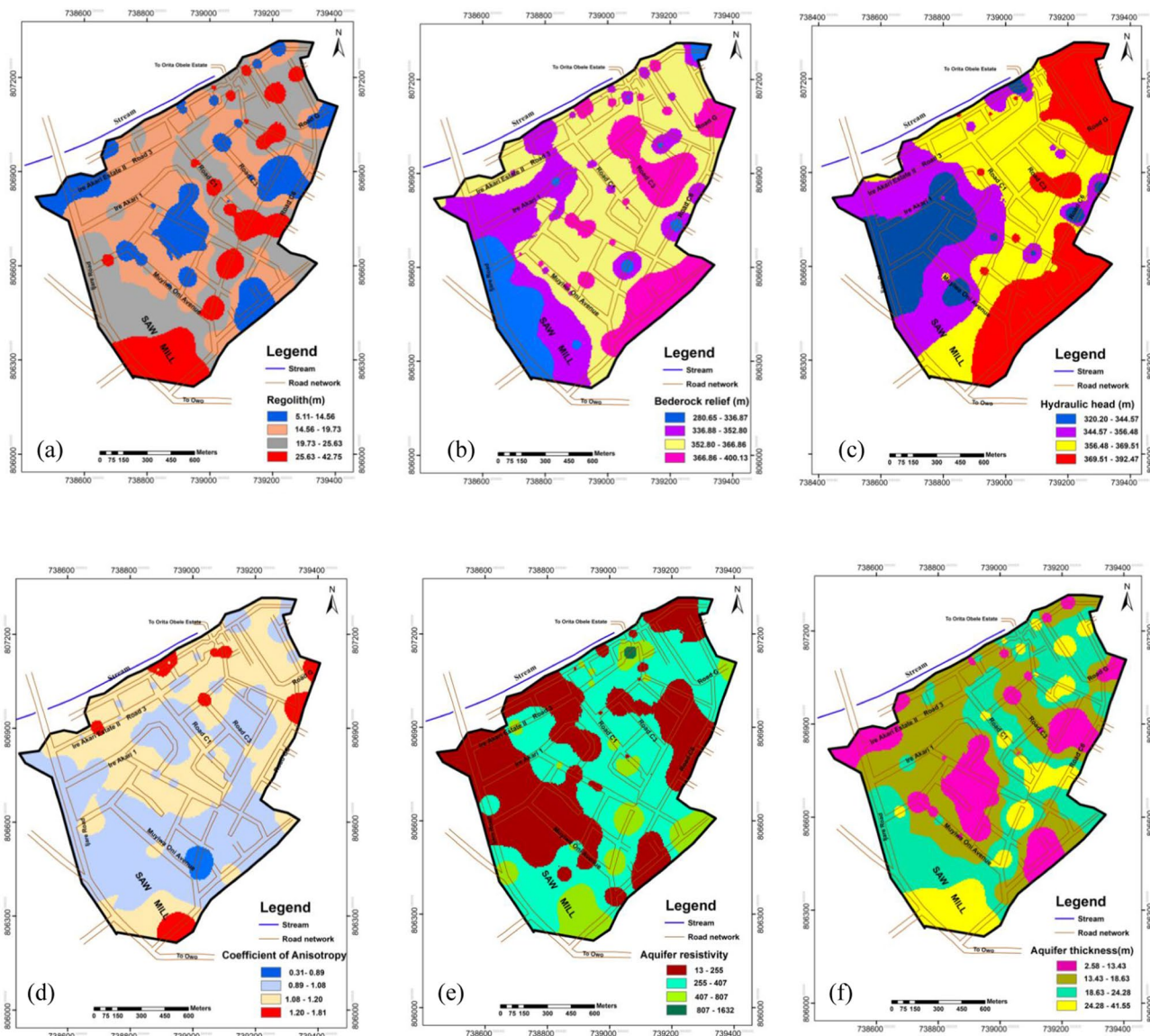


Fig. 7 The groundwater controlling factors themes: **a** regolith; **b** bedrock relief; **c** hydraulic head; **d** coefficient of anisotropy; **e** aquifer resistivity; **f** aquifer thickness

and 23–222 Ω m and 338–714 Ω m, respectively, delineated by the 2-D resistivity structures and the geoelectric sections constitute the aquifer units with hydrogeological significance in the investigated area.

The 1-D depth sounding and hydrogeological investigation results

The results of the interpreted 1-D depth sounding data were analyzed in terms of the distribution of the apparent resistivity and thicknesses values from which the earth subsurface models' strata/layers were delineated. The summary of the interpreted 1-D depth sounding and the hydrogeological

(well data) results are presented in Tables 1 and 2. Table 1 results were geoelectrically analyzed for lithologic layers delineation such as Regolith (*Re*), Bedrock relief (*B*), the aquifer unit's physical properties i.e. aquifer layer Resistivity (*R*) and aquifer layer Thickness (*T*). Furthermore, applying Eqs. 1 and 2 to Table 1 content, the coefficient of Anisotropy (λ) parameter “A” was determined. The *Re*, *B*, *A*, *R*, and *T* estimated values beneath each VES location are presented in Table 3. However, the “*H*” estimated values beneath each well are presented in column 7 of Table 2. According to Tables 2 and 3, the estimated values for *Re*, *B*, *H*, *A*, *R*, and *T* are in the range of 5.1–42.8 m, 198–30,040 m, 320.2–392.5 m, 0.31–1.83, 13–1641 Ω m and 2.5–41.6 m,

respectively. Tables 2 and 3 results were processed in a GIS environment to produce the thematic maps for the Hydrogeophysical geoelectrical-derived Groundwater Potential Conditioning Factors (GPCFs) (Fig. 5). Table 4 presents a summary of the geoelectric parameters beneath the study area.

The GPCFs weighting assignment result

The standard scale of Saaty’s developed in 1980 (Table 5) was adopted, coupled with the expert opinion gathered based on information answered in a keenly assessed questionnaire forms administered. Coupled with the intuitive knowledge of the researchers and analyzed assigned GPCFs weight from experts, the GPCFs multivariable criteria were compared for the study area groundwater potential assessment. Evolving from this criteria comparison was a pair-wise comparison matrix presented in Table 5. Adopting similar approaches reported in the studies of Jha et al. (2010), Akinlalu et al. (2017) and Mogaji and Lim (2017), etc., Table 5 was solved to determine the criterion normalized weight (NW). Applying Eqs. (6 and 7), the consistency of the criteria normalized weights were established. The result of the applied Eq. (7,) gives the consistency ratio (CR) of 0.05 (column 8 of Table 5). In accordance with Saaty (1980), if the $CR \leq 0.1$ (10%), then the CR is acceptable, implying that the matrix is consistent. Thus, the determined criteria normalized weights can be assigned to the considered GPCFs themes as shown in Table 6.

The groundwater potential prediction index (GPPI) model application results

The basic components of the developed GPPI algorithm (Eq. 9) are the normalized weight (NW) and assign rating (R) for the classes in each thematic maps (Fig. 5). These assigned NW and R have crucial hydrological implications considering that the NW component which gives insight to the relative importance of the GPCFs in contributing toward groundwater potential assessment in the area, while R defined the ranges of the aquifer expected productivity potential for groundwater storage interpretation based on the order of each factors map's class boundary influences. The quantitative analysis of the maps (Fig. 5) is presented in column 2 of Table 6. In a typical theme of the regolith (Re) factor (Fig. 5a), the class boundary with high Re values ranges of 25.63–42.75 m (column 2) is assigned the highest rating score of 4 (column 4 of Table 6). According to Oladapo et al. (2009), Mogaji (2016) and Bayode (2018), an area underlain with thicker Re unit is often observed to be characterized by high/medium groundwater yield. Thus, the aquifer expected productivity potential interpretation (Column 3 of Table 6) is in agreement. This trend is similar across the other GPCFs themes. Considering the GPCFs' weight (NW) assessment result in column 5 of Table 6 and the spatial attribute scoring values (R) based on the GIS designed template model (Fig. 8) on each GPCFs' themes, the developed GPPI multi-criteria modeling algorithm in Eq. (9) was explored for the groundwater potentiality index computation in the area. The GPPI modeling application result is presented in Table 7.

Table 5 A matrix of pair-wise comparisons of groundwater potential conditioning factors (GPCFs) for the AHP process

Pairwise comparison 9 point continuous rating scale										
Less important					More important					
1/9	1/7	1/5	1/3	1	3	5	7	9		
Extremely	Very strongly	Strongly	Moderately	Equally	Moderately	Strongly		Very strongly	Extremely	
			T	Re	R	B	H	A	NW	CR
T			1	3	3	5	9	1	0.3	0.05
Re			1/3	1	3	5	9	1/3	0.18	
R			1/3	1/3	1	3	5	1/5	0.1	
B			1/5	1/5	1/3	1	3	1/7	0.05	
H			1/9	1/9	1/5	1/3	1	1/9	0.03	
A			1	3	5	7	9	1	0.35	
Column total			2.97	7.64	12.53	21.33	36	2.78	1	

Re: **Regolith**; B: **Bedrock relief**; H: **Hydraulic head**; A: coefficient of Anisotropy; R: aquifer **Resistivity** and T: aquifer **Thickness**; GPCFs: Groundwater Potentiality Conditioning Factors; NW: Normalized Weight

Table 6 The probabilistic weightage scoring application to the GPCFs themes

GPCFsThemes	Category/class	Aquifer expected productivity potential	Rate <i>R</i>	NW
Re	5.12–14.56	Low	1	0.18
	14.56–19.73	Medium	2	
	19.73–25.63	Medium–high	3	
	25.63–42.76	High	4	
B	280.65–336.88	High	4	0.05
	336.88–352.81	Medium–high	3	
	352.81–366.86	Medium	2	
	366.86–400.13	Low	1	
H	320.20–344.57	High	4	0.03
	344.57–356.76	Medium–high	3	
	356.76–369.80	Medium	2	
	369.80–392.47	Low	1	
A	0.31–0.90	Low	1	0.35
	0.90–1.09	Medium	2	
	1.09–1.21	Medium–high	3	
	1.21–1.82	High	4	
R	13–255	High	4	0.1
	255–407	Medium–high	3	
	407–807	Medium	2	
	807–1632	Low	1	
T	2.58–13.43	Low	1	0.3
	13.43–18.63	Medium	2	
	18.63–24.28	Medium–high	3	
	24.28–41.55	High	4	

Re regolith, *B* bedrock relief, *H* hydraulic head, *A* coefficient of anisotropy, *R* aquifer resistivity, *T* aquifer thickness, *GPCFs* groundwater potentiality conditioning factors, *NW* normalized weight

Modeling of groundwater potentiality prediction zones (GPPZs) map

The estimated GPPI values resulting from the applied GPPI multi-criteria modeling equation (Eq. 9) are as presented in Table 7 (Column 9). The computed GPPI values for each grid center (Fig. 8) are noted to be a series of continuous values in the range of 1.59–3.65 for the study area. These GPPI record values were processed in a GIS environment to spatially model the groundwater potential prediction indexing (GPPI) map for the area (Fig. 9). For the potential zone demarcation, the appropriateness of the quantile classification method as applied in the studies of Razandi et al. (2015) and Rahmati and Melesse (2016) was employed. Table 8 presents the results of the potentiality zones' classification. Furthermore, the areal and percentage distribution of these predicted potential zones were evaluated in GIS environment and established that the coexisting percentage areas under Low (L), Medium (M), Medium–High (MH), and High (H)

categories are 24%, 47%, 22%, and 7%, respectively (Column 3 of Table 8).

Validation of the groundwater potential prediction index model map

The functionality of a regionalized model map for practical and field usage in any environmental impact assessment is of the essence in the field of groundwater hydrology (Mogaji 2016, 2017). According to Jha et al. (2010), the most appropriate approach for reliability assessment of a predictive model map is the step-draw down test at various locations within each predicted zones. With this approach, the location-specific safe aquifer yields would have been determined. But then, the non-availability of such data made this approach implementation difficult. Thus, well data record (Table 2) obtained via hydrogeological survey measurement were explored for the map model output's reliability evaluation. This approach is in agreement with the validation technique adopted in the studies of Manap et al. (2011) and Akinlalu et al. (2017), etc. This study engaged the Relative Operating Characteristic (ROC) technique, which can be highly efficient in examining the quality of deterministic and probabilistic detection and forecast systems for performance assessment of our produced GPPI model map. The appropriateness of the ROC technique proficiency in environmental decision-making analysis has been established in the studies of Al-abadi and Shahid (2015), Al-Abadi (2015) and Mogaji (2017). The basic mechanism of ROC for performance evaluation involving the use of ROC module of the IDRISI Selva software is explored in this study. It is important to note that the Depth to water level (DWL) records observed during wet seasons (Column 5 of Table 2) was considered as a training data used in preparing the GPPI model map while the Depth to water level (DWL) records observed at the peak of dry seasons (Column 6 of Table 2) not used in GPPI model map generation (Fig. 9) were used as testing data in GIS environment. The ROC curve application result is presented in (Fig. 9). Figure 9 shows that the success and prediction rates of the produced GPPI map are 0.855 (86%) and 0.812 (81%), respectively. According to Pradhan (2013), the uniqueness of the determined success rate is that it establishes the performance of resulting GPPI map (Fig. 9) in classifying the areas' existing wells, whereas the prediction rate describes the performance of the model and the predictor variable in anticipating the area groundwater occurrence. With these success and prediction accuracy results, the produced AHP-based GPPI map is reasonably suitable for decision-making to maximize groundwater resource development in the study area.

Furthermore, through overlaying the GPCFs' indices parameters' themes (Fig. 2) on the GPPI map (Fig. 9) in a GIS environment, further evaluation of the precision

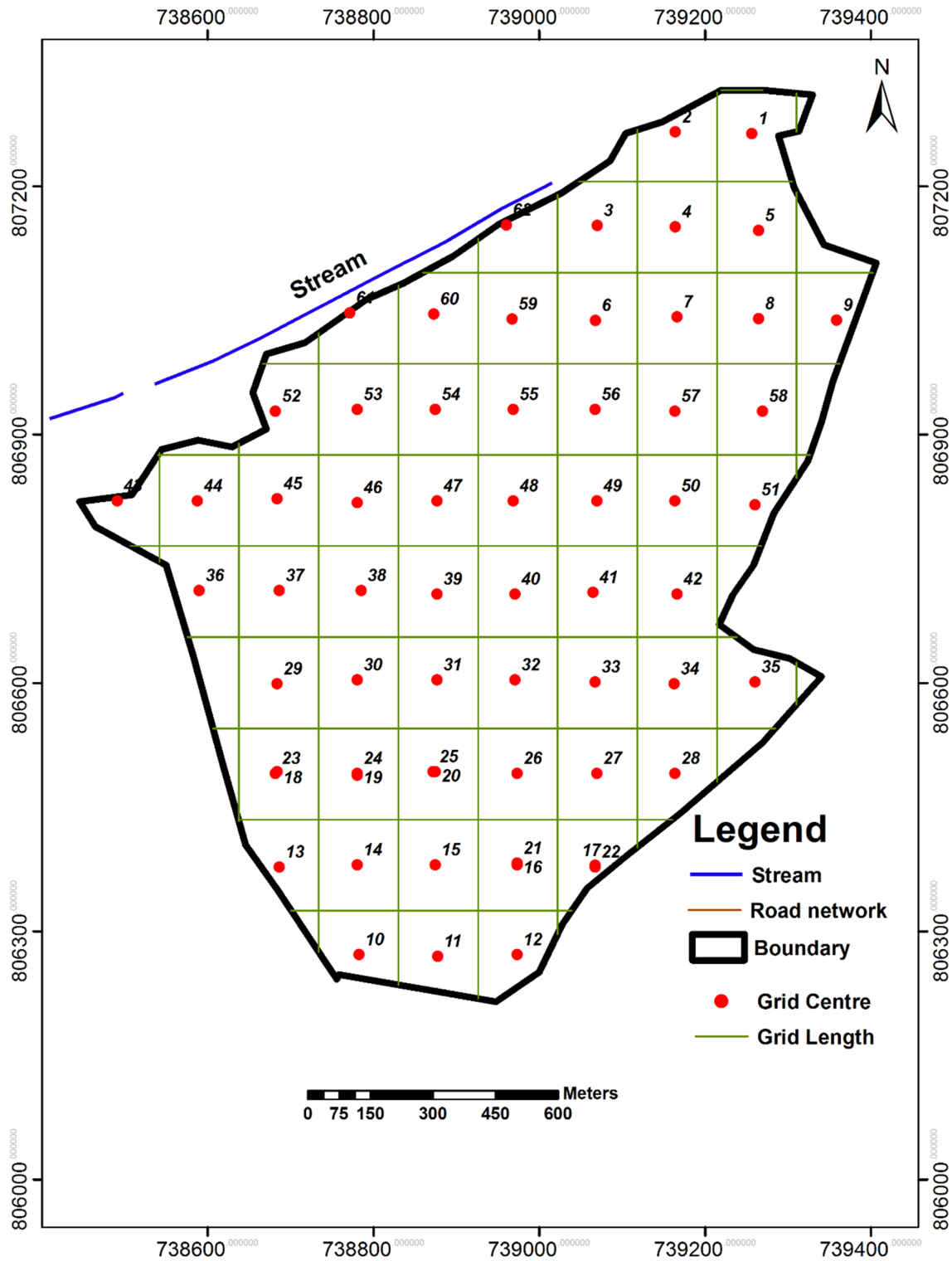


Fig. 8 GIS-based spatial attribute modeling template

prediction based on the proposed GIS-Based GPPI multi-criteria model was carried out. For the *Re*, *H*, *A*, *T* themes, a qualitative correlation assessment across the predicted potential zones i.e., from low to high, the medium–high

and high potential rate classified zones are correlated with the highest *Re*, *H*, *A*, *T* predicted values reducing down to the other classified zones (medium high, medium and low). Moreover, the medium–high and high groundwater potential

Table 7 The GIS-based developed GPPI model application results

<i>E</i>	<i>N</i>	<i>Re</i> (NW × <i>R</i>)	<i>b</i> (NW × <i>R</i>)	<i>h</i> (NW × <i>R</i>)	<i>a</i> (NW × <i>R</i>)	<i>r</i> (NW × <i>R</i>)	<i>t</i> (NW × <i>R</i>)	AWPI = $\sum NW_i \times R_i$
739,256.72	807,263.51	0.36	0.15	0.03	1.05	0.4	0.6	2.59
739,164.39	807,265.56	0.36	0.1	0.03	0.7	0.4	0.6	2.19
739,070.16	807,152.89	0.72	0.15	0.09	1.4	0.1	1.2	3.66
739,164.39	807,150.84	0.54	0.1	0.03	1.05	0.3	0.9	2.92
739,264.77	807,146.74	0.54	0.1	0.03	1.05	0.3	0.9	2.92
739,068.11	807,038.12	0.36	0.05	0.06	0.7	0.3	0.6	2.07
739,166.44	807,042.26	0.54	0.1	0.06	1.05	0.3	0.9	2.95
739,264.77	807,040.22	0.54	0.1	0.03	1.05	0.3	0.9	2.92
739,359.00	807,038.17	0.18	0.1	0.03	1.05	0.3	0.6	2.26
738,783.00	806,272.18	0.72	0.2	0.06	1.05	0.3	1.2	3.53
738,877.87	806,269.82	0.72	0.15	0.06	1.05	0.2	1.2	3.38
738,973.49	806,272.18	0.72	0.1	0.03	1.4	0.2	1.2	3.65
738,686.57	806,378.00	0.54	0.2	0.09	0.7	0.3	0.9	2.73
738,780.65	806,380.36	0.54	0.15	0.09	0.7	0.3	0.9	2.68
738,874.72	806,380.36	0.72	0.15	0.06	0.7	0.2	1.2	3.03
738,973.49	806,380.36	0.54	0.1	0.03	0.7	0.3	0.9	2.57
739,067.56	806,380.00	0.36	0.05	0.03	0.7	0.3	0.6	2.04
738,684.23	806,493.24	0.54	0.2	0.12	0.7	0.3	0.9	2.76
738,780.65	806,488.54	0.54	0.2	0.09	0.7	0.4	0.9	2.83
738,874.72	806,493.24	0.54	0.1	0.12	1.05	0.3	0.6	2.71
738,973.48	806,490.89	0.54	0.1	0.03	0.35	0.3	0.9	2.22
739,069.91	806,490.89	0.36	0.05	0.03	0.7	0.3	0.6	2.04
739,163.98	806,490.89	0.18	0.05	0.03	0.7	0.4	0.3	1.66
738,684.23	806,599.07	0.54	0.2	0.12	1.05	0.4	1.2	3.51
738,780.65	806,603.77	0.18	0.05	0.09	0.7	0.4	0.3	1.72
738,877.07	806,603.77	0.36	0.1	0.09	0.7	0.4	0.3	1.95
738,971.14	806,603.77	0.36	0.1	0.06	0.7	0.3	0.6	2.12
739,067.56	806,601.42	0.72	0.2	0.06	0.7	0.2	1.2	3.08
739,163.18	806,599.07	0.36	0.1	0.06	0.7	0.3	0.6	2.12
739,260.40	806,601.42	0.54	0.05	0.03	0.7	0.2	0.9	2.42
738,590.16	806,711.95	0.36	0.15	0.12	0.7	0.4	0.6	2.33
738,686.58	806,711.75	0.36	0.15	0.12	0.7	0.4	0.6	2.33
738,785.35	806,711.95	0.36	0.1	0.12	1.05	0.4	0.6	2.63
738,877.07	806,707.25	0.18	0.1	0.12	1.05	0.4	0.3	2.15
738,971.14	806,707.25	0.18	0.1	0.09	1.05	0.4	0.3	2.12
739,065.21	806,709.60	0.54	0.1	0.06	1.05	0.3	0.9	2.95
739,166.33	806,707.25	0.72	0.1	0.03	0.7	0.3	1.2	3.05
738,491.38	806,820.13	0.18	0.15	0.09	0.7	0.4	0.3	1.82
738,587.80	806,820.13	0.18	0.15	0.09	0.7	0.4	0.3	1.82
738,684.23	806,822.48	0.36	0.15	0.09	1.05	0.4	0.6	2.65
738,780.65	806,817.78	0.36	0.1	0.12	1.05	0.3	0.6	2.53
738,877.08	806,820.13	0.36	0.1	0.09	1.05	0.3	0.6	2.5
738,968.79	806,820.13	0.36	0.1	0.09	0.7	0.4	0.6	2.25
739,069.91	806,820.13	0.36	0.05	0.06	0.7	0.3	0.6	2.07
739,163.98	806,820.13	0.18	0.05	0.06	0.7	0.3	0.3	1.59
739,260.40	806,815.43	0.36	0.15	0.09	1.05	0.4	0.6	2.65
738,682.23	806,928.31	0.36	0.1	0.09	1.05	0.3	0.6	2.5
738,780.65	806,930.66	0.36	0.1	0.09	1.05	0.3	0.6	2.5
738,874.72	806,930.66	0.36	0.15	0.06	0.7	0.4	0.6	2.27
738,968.79	806,930.66	0.54	0.1	0.06	0.7	0.3	1.2	2.9

Table 7 (continued)

<i>E</i>	<i>N</i>	<i>Re</i> (NW × <i>R</i>)	<i>b</i> (NW × <i>R</i>)	<i>h</i> (NW × <i>R</i>)	<i>a</i> (NW × <i>R</i>)	<i>r</i> (NW × <i>R</i>)	<i>t</i> (NW × <i>R</i>)	AWPI = $\sum NW_i \times R_i$
739,067.56	806,930.66	0.36	0.1	0.06	1.05	0.3	0.6	2.47
739,163.98	806,928.31	0.36	0.05	0.06	0.7	0.4	0.6	2.17
739,269.81	806,928.31	0.18	0.05	0.06	1.05	0.4	0.3	2.04
738,967.82	807,039.76	0.54	0.1	0.06	1.05	0.3	0.9	2.95
738,873.23	807,045.85	0.36	0.1	0.09	0.7	0.4	0.6	2.25
738,771.55	807,046.85	0.54	0.15	0.06	1.05	0.4	0.6	2.8
738,960.73	807,153.26	0.36	0.1	0.09	1.05	0.4	0.6	2.6

Re regolith, *B* bedrock relief, *H* hydraulic head, *A* coefficient of anisotropy, *R* aquifer resistivity, *T* aquifer thickness, *E* and *N* the attributes' grid center's coordinate

classes mainly cover the southern, western and extend to the northern parts, with two smaller isolated areas observed in the eastern part of the study areas and these areas are typically underlain with saturated aquifer formation (*R*) (Fig. 5e, f) and relatively low bedrock relief zones (*B*) (Fig. 5b). In line with Omosuyi et al. (2007), Oladapo et al. (2009), Bayode (2018) and Adagunodo et al. (2018), zones characterized with saturated aquifer formation and low bedrock relief i.e., a depression zone often served as groundwater collecting center and are zones of high groundwater potential zone in a typical crystalline rock area. The correlation of (Fig. 9) spatial attribute prediction output with these aforementioned GPCFs further substantiates the appropriateness of the proposed GIS-Base GPPI multi-criteria model in environmental decision-making studies.

Conclusions

This study has successfully explored the efficacy of geospatial tool in modeling the geophysically/hydrogeological derived groundwater potentiality conditioning factors (GPCFs) such as regolith thickness, bedrock relief, hydraulic head, coefficient of anisotropy, aquifer resistivity, and aquifer thickness toward groundwater potentiality assessment in the study area. The data sources for the derived GPCFs include the 2-D, 1-D geophysical imaging data and hydrogeological well data acquired in a typical hard rock terrain. Through robust analysis of the geophysical data using appropriate software, geoelectrical parameters were determined. The interpreted geoelectric parameters enable subsurface lithological imaging of geologic features including major vertical discontinuities characterized by relatively low resistivity zones within the highly resistive basement bed rock (between distances > 370 m; 480–530 m; 180–220 m; 90–120 m along the established 2-D resistivity

imaging traverses (1, 2, 5 and 6, respectively) typical of the delineated fracture zones that are of hydrogeological significance in the investigated area. The reprocessing of these geoelectrical parameters (resistivity and thickness) lead to the establishment of Dar-Zarrouk Parameters. The hydrogeological well data and the primary and secondary geoelectric parameters were processed in a GIS environment to obtain the area groundwater potentiality conditioning factors 'themes. Applying the standard Saaty's scale in the context of analytical hierarchy process (AHP) data mining approach, the rated and weighted thematic layers were integrated in GIS environment to compute groundwater potential prediction index (GPPI) for the area. Based on the results of the estimated GPPI in the range of between 1.59 and 3.65, the study area was classified into four groundwater potential zones. The map revealed that about 71% of the areal extent accounts for the low, and medium predicted groundwater potential classes and 29% of the area covers the moderate-high to high groundwater potential classes. The reliability evaluation of the produced GPPI map was investigated using the Reacting Operating Characteristics (ROC) success and prediction rates deterministic approach. The success and the prediction rates for the produced GPPI map are 0.855 and 0.812, respectively. Besides, the precise correlation of this GIS-Base GPPI multi-criteria model map with the GPCFs themes' spatial attributes output further substantiates its appropriateness in environmental decision-making studies. Thus, information on the produced GPZM could be used by local authorities and water policy makers as a preliminary reference in selecting suitable sites for drilling new boreholes. The findings affirmed the identification of areas where aquifers can be developed. The research output will greatly contribute to the precise location of borehole site that could address the groundwater resources development challenges in the investigated area and another area with similar geology.

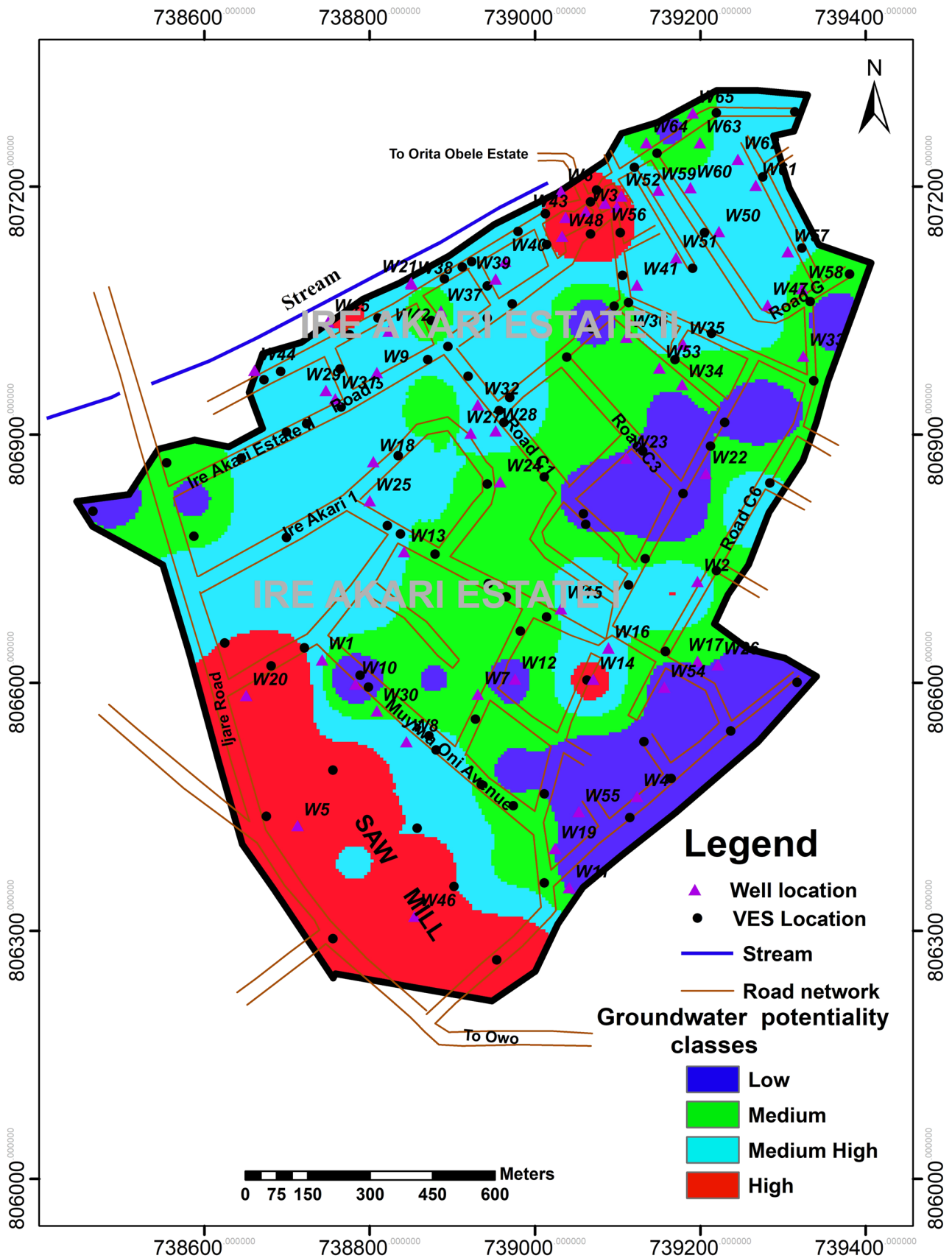


Fig. 9 Groundwater potentiality zonation map (GPZM) of the study area

Table 8 The potentiality classifications based on the applied GPPI model equation

Potential index classification	Model map analysis		DWL analysis
	Range	Areal (%)	
L	1.59–2.30	24	3.27
M	2.30–2.61	47	5.51
MH	2.61–3.02	22	7.36
H	3.02–3.66	07	8.76

L low, *M* medium, *MH* medium high, *H* high, *DWL* depth to water level

Acknowledgements The authors are grateful to Mr. P. Edugbe, Mr. A. A. Badmus, Mr. F. Aiwekohe, Mr. T. Adewumi, and Mr. A. Adewale who assisted with the fieldwork.

Funding There is no funding for this research. It was sponsored by the authors from personal income.

Declarations

Conflict of interest There is no conflict of interest whatsoever.

Ethical conduct The study complied with all ethical guidelines.

Open Access This article is licensed under a Creative Commons Attribution 4.0 International License, which permits use, sharing, adaptation, distribution and reproduction in any medium or format, as long as you give appropriate credit to the original author(s) and the source, provide a link to the Creative Commons licence, and indicate if changes were made. The images or other third party material in this article are included in the article's Creative Commons licence, unless indicated otherwise in a credit line to the material. If material is not included in the article's Creative Commons licence and your intended use is not permitted by statutory regulation or exceeds the permitted use, you will need to obtain permission directly from the copyright holder. To view a copy of this licence, visit <http://creativecommons.org/licenses/by/4.0/>.

References

- Abdulla FA, Al-Shareef AW (2009) Roof rainwater harvesting systems for household water supply in Jordan. *Desalination* 243(1–3):195–207
- Acharya T, Kumbhakar S, Prasad R, Surajit M, Arkoprovo B (2017) Delineation of potential groundwater recharge zones in the coastal area of north-eastern India using geoinformatics. *Sustain Water Resour Manag*. <https://doi.org/10.1007/s40899-017-0206-4>
- Adagunodo TA, Margaret KA, Sunmonu LA, Aizebeokhai AP, Oyeyemi KD, Abodunrin FO (2018) Groundwater exploration in Aaba residential area of Akure, Nigeria. *Front Earth Sci*. <https://doi.org/10.3389/feart.2018.00066>
- Adiat KAN, Nawawi MNM, Abdullah K (2012) Assessing the accuracy of GIS-based elementary multi criteria decision analysis as a spatial prediction tool—a case of predicting potential zones of sustainable groundwater resources. *J Hydrol* 440:75–89. <https://doi.org/10.1016/j.jhydrol.2012.03.028>
- Adiat KAN, Nawawi MNM, Abdullah K (2013) Application of multi-criteria decision analysis to geoelectric and geologic parameters for spatial prediction of groundwater resources potential and aquifer evaluation. *Pure Appl Geophys* 170:453–471. <https://doi.org/10.1007/s00024-012-0501-9>
- Akinlalu AA, Adegbuyiro A, Adiat KAN, Akeredolu BE, Lateef WY (2017) Application of multi-criteria decision analysis in prediction of groundwater resources potential: a case of Oke-Ana, Ilesa Area Southwestern Nigeria. *NRIAG J Astron Geophys* 6:184–200
- Al Saud M (2010) Mapping potential areas for groundwater storage in Wadi Aurnah Basin, western Arabian Peninsula, using remote sensing and geographic information system techniques. *Hydrogeol J* 18:1481–1495
- Al-Abadi AM (2015) The application of Dempster–Shafer theory of evidence for assessing groundwater vulnerability at Galal Badra basin, Wasit governorate, east of Iraq. *Appl Water Sci*. <https://doi.org/10.1007/s13201-015-0342-7>
- Al-Abadi AM, Shahid S (2015) A comparison between index of entropy and catastrophe theory methods for mapping groundwater potential in an arid region. *Environ Monit Assess* 187:576. <https://doi.org/10.1007/s10661-015-4801-2>
- Al-Abadi AM, Shahid S (2016) GIS-based integration of catastrophe theory and analytical hierarchy process for mapping flood susceptibility: a case study of the Teeb area, Southern Iraq. *Environ Earth Sci* 75:687. <https://doi.org/10.1007/s12665-016-5523-7>
- Bala AN, Ike EC (2001) The aquifer of the crystalline basement rocks in Gusau area, North-western Nigeria. *J Min Geol* 37(2):177–184
- Bayode S (2013) Hydro-geophysical investigation of the Federal Housing Estate Akure, Southwestern Nigeria. *J Eng Trends Eng Appl Sci (JETEAS)* 4(6):793–799
- Bayode S (2018) A geoelectric investigation of the groundwater potential in a typical basement complex terrain of southwestern Nigeria. *J Earth Atmos Res* 1(1):42–50
- Bayode S, Akpoarebe O (2011) An integrated geophysical investigation of a spring in Ibuji, Igbara-Oke, Southwestern Nigeria. *IFE J Sci* 13(1):63–74
- Bayode S, Dogo TY, Jonibola O (2017) Groundwater potential evaluation in a typical hardrock terrain using GRRAT index model. *Int J Res Appl Nat Soc Sci IMPACT IJRANSS* 5(5):1–10
- Chowdhury A, Jha MK, Chowdary VM, Mal BC (2009) Integrated remote sensing and GIS-based approach for assessing groundwater potential in West Medinipur district, West Bengal, India. *Int J Remote Sens* 30(1):231–250
- Chowdhury A, Madan KJ, Chowdary VM (2010) Delineation of groundwater recharge zones and identification of artificial recharge sites in West Medinipur district, West Bengal, using RS, GIS and MCDM techniques. *Environ Earth Sci* 59:1209
- De Araujo CC, Macedo AB (2002) Multicriteria geologic data analysis for mineral favorability mapping: application to a metal sulphide mineralized area, Ribeira Valley Metallogenic Province, Brazil. *Nat Resour Res* 11(1):29–43
- Dipro for Windows (2000) DiproTM version 4.0 processing and interpretation software for dipole–dipole electrical resistivity data. KIGAM, Daejeon
- Eastman JR (1996) Multi-criteria evaluation. In: Longley PA, Goodchild MF, Magurie DJ, Rhind DW (eds) *Geographical information systems*, vol 1, 2nd edn. Wiley, New York, pp 493–502
- Feizizadeh B, Blaschke T (2013) GIS-multicriteria decision analysis for landslide susceptibility mapping: comparing three methods for the Urmia lake basin, Iran. *Nat Hazards* 65:2105–2128. <https://doi.org/10.1007/s11069-012-0463-3>
- Fetter CW (1994) *Applied hydrogeology*, 4th edn. Prentice Hall, Englewood Cliffs, pp 543–591
- Garfi M, Tondelli S, Bonoli A (2009) Multi-criteria decision analysis for waste management in Saharawi refugee camps. *Waste Manag* 29:2729–2739
- Ge S, Gorelick SM (2015) *Groundwater and surface water*. Elsevier, Amsterdam

- George M, Ogendi A, Isaac M (2009) Ong'oa. In: Water policy, accessibility and water ethics in Kenya, 7 Santa Clara J. *Int'l L.* 177. Available at: <http://digitalcommons.law.scu.edu/scujil/vol7/iss1/3>
- Graham-Tomasl T, Yacov T (2004) The buffer value of groundwater with stochastic surface water supplies. *J Environ Econ Manag* 21(3):201–224
- Jha M, Chowdary V, Chowdhury A (2010) Groundwater assessment in Salboni Block, West Bengal (India) using remote sensing, geographical information system and multi-criteria decision analysis techniques. *Hydrogeol J* 18:1713–1728. <https://doi.org/10.1007/s10040-010-0631-z>
- Keller GV, Frischnecht FC (1966) *Electrical methods in geophysical prospecting*. Pergamon Press, Oxford, p 523
- Lewis MA (1990) The analysis of borehole yields from basement aquifer. Commonwealth Science Council, Technical Paper, London, 273(2):171–202
- Machiwal D, Rangi N, Sharma A (2015) Integrated knowledge- and data-driven approaches for groundwater potential zoning using GIS and multi-criteria decision making techniques on hard-rock terrain of Ahar catchment, Rajasthan, India. *Environ Earth Sci* 73:1871–1892
- Madan KJ, Chowdary VM, Chowdhury A (2010) Groundwater assessment in Salboni Block, West Bengal (India) using remote sensing, geographical information system and multi-criteria decision analysis techniques. *Hydrogeol J* 18(7):1713–1728
- Magesh NS, Chandrasekar N, Soundranayagam JP (2012) Delineation of groundwater potential zones in Theni district, Tamil Nadu, using remote sensing, GIS and MIF techniques. *Geosci Front* 3(2):189–219
- Malczewski J (2006) Ordered weighted averaging with fuzzy quantifiers: GIS-based multi-criteria evaluation for land-use suitability analysis. *Int J Appl Earth Obs Geoinf* 8:270–277
- Malczewski J, Rinner C (2005) Exploring multicriteria decision strategies in GIS with linguistic quantifiers: a case study of residential quality evaluation. *J Geogr Syst* 7:249–268
- Manap MA, Sulaiman WNA, Ramli MF, Pradhan B, Surip N (2011) A knowledge-driven GIS modeling technique for groundwater potential mapping at the Upper Langat Basin, Malaysia. *Arab J Geosci* 6:1621–1637. <https://doi.org/10.1007/s12517-011-0469-2>
- Marsalek J, Jiménez-Cisneros BE, Malmquist PA, Karamouz M, Goldenfum J, Chocat B (2006) *Urban water cycle processes and interactions*. Technical documents in hydrology No. 78 UNESCO, Paris
- Mogaji KA (2016) Combining geophysical techniques and multi-criteria GIS-based application modeling approach for groundwater potential assessment in southwestern Nigeria. *Environ Earth Sci* 75:1181. <https://doi.org/10.1007/s12665-016-5897>
- Mogaji KA (2017) Development of AHPDST vulnerability indexing model for groundwater vulnerability assessment using hydrogeophysical derived parameters and GIS application. *Pure Appl Geophys*. <https://doi.org/10.1007/s00024-017-1499-9>
- Mogaji KA, Lim HS (2017) Groundwater potentiality mapping using geoelectrical based aquifer hydraulic parameters: a GIS-based multi-criteria decision analysis modeling approach *Terr. Atmos Ocean Sci* 28(3):479–500. <https://doi.org/10.3319/TAO.2016.11.01.02>
- Mogaji KA, Lim HS (2018) Application of Dempster–Shafer theory of evidence model to geoelectric and hydraulic parameters for groundwater potential zonation. *NRIAG J Astron Geophys* 7(2018):134–148. <https://doi.org/10.1016/j.nrjag.2017.12.008>
- Mukherjee S, Zankhana S, Kumar MD (2009) Sustaining urban water supplies in India: increasing role of large reservoirs. *Water Resour Manag* 24:2035–2055. <https://doi.org/10.1007/s11269-009-9537-8>
- Nampak H, Pradhan B, Manap MA (2014) Application of GIS based data driven evidential belief function model to predict groundwater potential zonation. *J Hydrol* 513:283–300
- NIMETS (2011) Nigerian Meteorological Agency
- Oborie E, Udom GJ (2014) Determination of aquifer transmissivity using geoelectrical sounding and pumping test in parts of Bayelsa State, Nigeria. *Peak J Phys Environ Sci Res* 2:32–40
- Oikonomidis D, Dimogianni S, Kazakis N, Voudouris KA (2015) GIS/remote sensing-based methodology for groundwater potentiality assessment in Tirnavos area, Greece. *J Hydrol* 525:197–208
- Ojo JS, Olorunfemi MO, Akintorinwa OJ, Bayode S, Omosuyi GO, Akinluyi FO (2015) GIS Integrated Geomorphological, geological and geoelectrical assessment of the groundwater potential of Akure metropolis, southwest Nigeria. *J Earth Sci Geotech Eng* 5(14):85–101
- Oladapo MI, Adeoye OO, Mogaji KA (2009) Hydrogeophysical study of the groundwater potential of Ilara–Mokin southwestern, Nigeria. *Glob J Earth Sci* 15(2):195–204
- Olorunfemi MO, Olarewaju VO, Alade O (1991) On the electrical anisotropy and groundwater yield in a basement complex area of S. W. Nigeria. *J Afr Earth Sci* 12(3):467–472
- Olorunfemi MO, Ojo JS, Akintunde OM (1999) Hydro-geophysical evaluation of the groundwater potentials of the Akure, Metropolis, southwestern Nigeria. *J Min Geol* 35(2):207–226
- Omosuyi GO, Adeyemo A, Adegoke AO (2007) Investigation of groundwater prospecting using electromagnetic and geoelectric sounding at Afunbiowo, near Akure, southwestern Nigeria. *Pac J Sci Technol* 8(2):172–181
- Omosuyi GO, Oseghale A, Bayode S (2013) Hydrogeophysical delineation of groundwater prospect zones at Odigbo, Southwestern Nigeria. *Acad J* 8(15):596–608
- Pham BT, Prakash I, Dou J, Singh SK, Trinh PT, Tran HT, Le TM, Van Phong T, Khoi DK, Shirzadi A (2019) A novel hybrid approach of landslide susceptibility modelling using rotation forest ensemble and different base classifiers. *Geocarto Int* 35:1–25
- Pradhan B (2013) A comparative study on the predictive ability of the decision tree, support vector machine and neuro-fuzzy models in landslide susceptibility mapping using GIS. *Comput Geosci* 51:350–365. <https://doi.org/10.1016/j.cageo.2012.08.023>
- Rahaman MA (1976) *A review of the basement geology of southwestern Nigeria in geology of Nigeria*. Elizabethan Publishing Company Nigeria, Lagos, pp 41–58
- Rahmati O, Melesse AM (2016) Application of Dempster–Shafer theory, spatial analysis and remote sensing for groundwater potentiality and nitrate pollution analysis in the semi-arid region of Khuzestan, Iran. *Sci Total Environ* 568:1110–1123. <https://doi.org/10.1016/j.scitotenv.2016.06.176>
- Razandi Y, Pourghasemi HR, Najmeh SN, Omid R (2015) Application of analytical hierarchy process, frequency ratio, and certainty factor models for groundwater potential mapping using GIS. *Earth Sci Inform* 8(4):867–883
- Roscoe Moss Co (1990) *Handbook of ground water development*. Wiley, New York, pp 34–51
- Saaty TL (1980) *The analytic hierarchy process: planning, priority setting, resource allocation*, McGraw-Hill, New York, p 287
- Satpathy BN, Kanungo BN (1976) Groundwater exploration in hard rock terrain—a case study. *Geophys Prospect* 24(4):725–763
- Thirumalaivasan D, Karmegam M, Venugopal K (2003) AHP-DRASTIC: software for specific aquifer vulnerability assessment using DRASTIC model and GIS. *Environ Model Softw* 18:645–656
- Tizro AT, Voudouris KS, Salehzade M, Mashayekhi H (2010) Hydrogeological framework and estimation of aquifer hydraulic parameters using geoelectrical data: a case study from West Iran. *Hydrogeol J* 18:917–929. <https://doi.org/10.1007/s10040-010-0580-6>

- Todd DK (1980) Groundwater hydrology, 2nd edn. Wiley, New York, pp 111–163
- Todd DK, Mays LW (2005) Groundwater hydrology. Wiley, New York
- UNESCO, UNESCO-WSSM (2019) Water security and the sustainable development goals (Series I). Global water security issues (GWSI) series. UNESCO Publishing, Paris
- Vahidnia MH, Alesheikh A, Alimohammadi (2009) Hospital site selection using fuzzy AHP and its derivatives. *J Environ Manag* 90:3048–3056. <https://doi.org/10.1016/j.jenvman.2009.04.010>
- Vander-Velper BPA (2004) Winresist version 1.0 resistivity depth sounding interpretation software. MSc research project, ITC, Delft
- Vörösmarty CJ, McIntyre PB, Gessner MO, Gessner D, Liermann RC, Davies PM (2010) Global threats to human water security and river biodiversity. *Nature* 467:555–561. <https://doi.org/10.1038/nature09549>